[American Journal of Science, Vol. 314, February, 2014, P. 613–648, DOI 10.2475/02.2014.06]

THE 186 MA DASHIBALBAR ALKALINE GRANITOID PLUTON IN THE NORTH-GOBI RIFT OF CENTRAL MONGOLIA: EVIDENCE FOR MELTING OF NEOPROTEROZOIC BASEMENT ABOVE A PLUME

J. DOSTAL*,†, J. V. OWEN*, O. GEREL**, J. D. KEPPIE***, R. CORNEY*, J. G. SHELLNUTT§, and A. MacRAE*

ABSTRACT. The Jurassic Dashibalbar granitoid pluton (~300 km^2) crops out in the Triassic North-Gobi rift of central Mongolia, just south of the 230 to 195 Ma Khentei batholith. The granitoids are shallow-seated dominantly, amphibole-bearing alkali feldspar granite that contain quartz-syenite/syenite enclaves. They are all composed of megacrystic mesoperthite, quartz, Ca-Na amphibole altered to biotite and rarely with pyroxene cores, magnetite and ilmenite. The pluton yielded a concordant U-Pb zircon age of 186 ± 1 Ma, which is similar to a published 189 ± 3 Ma $^{40}Ar/^{39}Ar$ amphibole age, and indicates rapid cooling through *ca.* 550 °C. This age is *ca.* 10 my younger than the 196 ± 4 Ma age of the bimodal volcanic complex intruded by the pluton. The volcanic complex is composed of augite-phyric transitional basalt and rhyolite/comendite. Both basalts and rhyolites/comendites are evolved within-plate varieties with positive $\varepsilon_{Nd(t)}$ (~ +2.5) values. The granitoids are evolved alkaline, A-type granites and quartz-syenites/syenites that are enriched in light REE's, but show a distinct depletion in Eu, Sr and Ba, indicative of feldspar fractionation. The data are consistent with derivation of the granites from the syenites by an assimilation-fractional crystallization process involving a silicic crustal contaminant. The granitic rocks have $\varepsilon_{Nd(t)}$ values of ~ +0.8 to +1.2, which are slightly lower than $\varepsilon_{Nd(t)}$ values +1.3 to +1.6 in the syenites, although both have similar T_{DM} model ages (~800-970 Ma). The ~800 Ma model ages of the basalt and rhyolite/comendite are comparable to those of the intrusion and enclaves. The compositions of all these rocks, including $\varepsilon_{Nd(t)}$ and T_{DM}, are within the range of A-type granites and volcanic complexes of the Early Mesozoic Mongolian-Transbaikalian igneous province. The results suggest derivation of a parent magma of the granitoids and felsic volcanic rocks from underplated, enriched, Neoproterozoic mantle-derived basaltic rocks in the lower crust, whereas the Dashibalbar basalts were derived from Neoproterozoic subcontinental lithospheric mantle; Neoproterozoic megablocks crop out in adjacent parts of the Central Asian Orogenic Belt. Melting of lower crust and subcontinental lithospheric mantle implies a rising heat source. Although such a heat source is consistent with both rifting and passage over the Mongolian mantle plume, only the latter explains the west-to-east migration of the magmatism and rifting.

Key words: A-type granite, mantle plume, rifting, Central Asian Orogenic belt, Jurassic, geochemistry

INTRODUCTION

The Mesozoic North-Gobi rift forms one of a series of rifts superimposed on the Paleozoic Central Asian Orogenic Belt (fig. 1) (CAOB: Sengör and others, 1993; Wilhen and others, 2012). A large number of the Mesozoic alkaline (A-type) granitoids, which are emplaced in these rifts, are spatially and temporally associated with a bimodal basalt-comendite/rhyolite suite. Granitoids of the CAOB have been interpreted in terms of rifting (Yarmolyuk and Kovalenko, 1991), delamination of the

* Department of Geology, Saint Mary's University, Halifax, Nova Scotia B3H 3C3, Canada
** Department of Geology and Mineralogy, Mongolian University of Science and Technology, P.O. Box 46/672, Ulaanbaatar, Mongolia
*** Instituto de Geologia, Universidad Nacional Autonoma de Mexico, 04510 Mexico D.F., Mexico
§ Department of Earth Science, National Taiwan Normal University, 88 Tingzhou Road Section 4, Taipei 11677, Taiwan (email: jgshelln@ntnu.edu.tw)
† Corresponding author: Tel: 902-420-5747; e-mail: jdostal@smu.ca

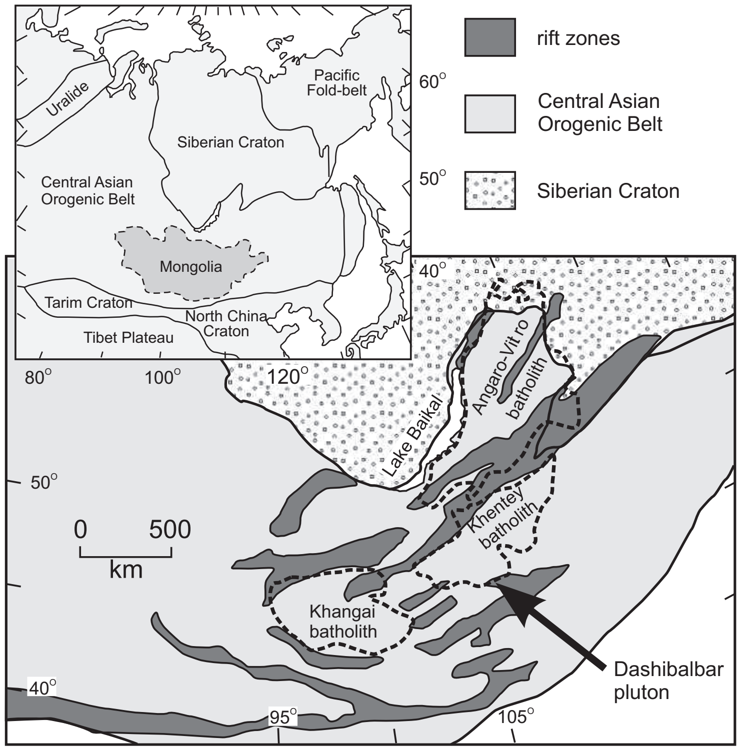

Fig. 1. Geological sketch map of the western part of the Central Asian Orogenic Belt showing the distribution of the Early Mesozoic rift zones (modified after Yarmolyuk and Kuzmin, 2011, and Jahn and others, 2009). Inset map shows a sketch of Central Asia Orogenic Belt and surrounding provinces (after Jahn and others, 2009).

CAOB root leading to upwelling of the asthenosphere (Wu and others, 2002), and a mantle plume (Yarmolyuk and Kuzmin, 2011). This mirrors the world-wide debate on the origin of A-type granitoids.

The A-type granites are a group of granitoid rocks with distinct but varied chemistry. They range in composition from syenogranites through peralkaline and alkali feldspar-rich granites to topaz granites (for example Whalen and others, 1987; Eby, 1992; Bonin, 2007). They are widespread, and many typically occur as volumetrically small intrusions with high concentrations of rare elements such as rare earth elements (REE), niobium, thorium and uranium, which occasionally are economically significant. Although these alkali- and iron-rich granites are widely reported in geological literature, their origin, evolution and tectonic setting are still being debated (for example Eby, 1990, 1992; Bonin, 2007; Jahn and others, 2009; Frost and Frost, 2011 and references therein). Eby (1992) subdivided A-type granites into two groups that differ in their tectonic significance. A1-type comprises anorogenic, mantle-derived granitoid rocks, whereas A2-type granites were emplaced in a variety of tectonic settings and were derived by melting of continental crust or underplated mafic crust. The generation of A-type granites requires a high melting temperature (Clemens and others, 1986), which can be produced by emplacement of mantle-derived mafic magma related to either upwelling of asthenosphere during rifting, slab break-off or delamination of thickened lithosphere. Several of petrogenetic models have been invoked for the genesis of A-type granites, including (1) differentiation of mantle-

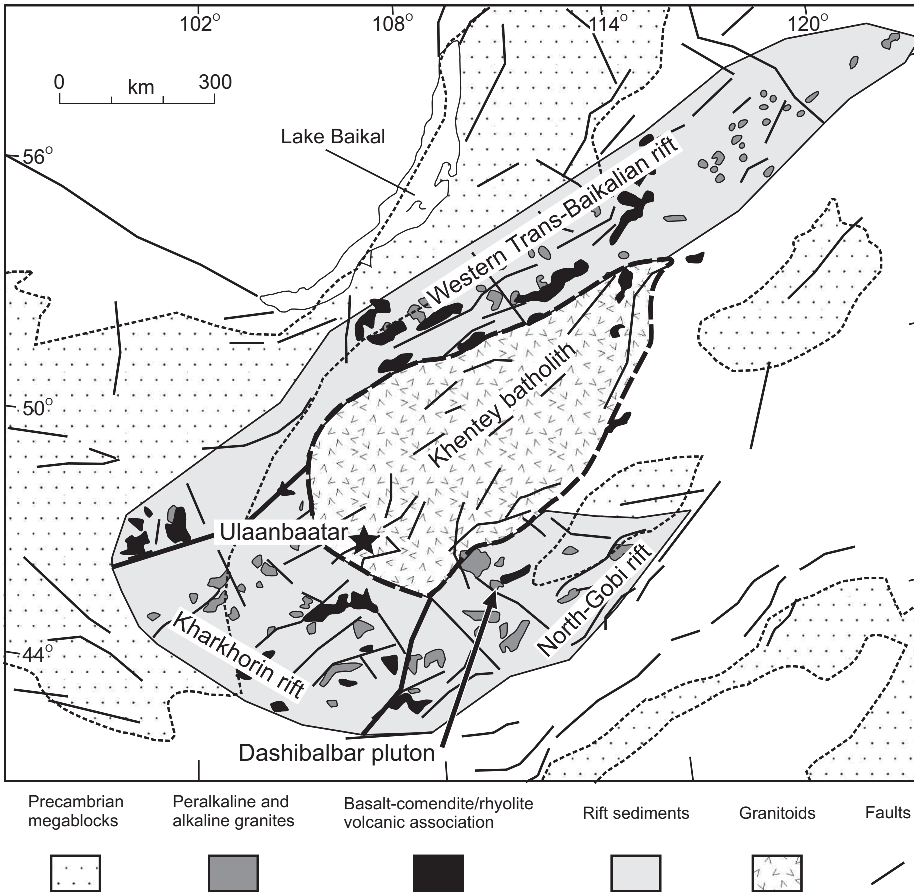

Fig. 2. Geological sketch map of central part of the Early Mesozoic Mongolian-Transbaikalian igneous province of the CAOB showing the Mesozoic North-Gobi, Western-Trans-Baikalian and Kharkhorin (Karakorum) rifts, Khentey batholith (modified after Yarmolyuk and others, 2002; Reichow and others, 2010; and Yarmolyuk and Kuzmin, 2011) and the Dashibalbar igneous complex.

derived mafic magmas (for example Eby, 1990; Turner and others, 1992); (2) interaction of mantle-derived magma with overlying crustal rocks (for example Kerr and Fryer, 1993), (3) partial melting of middle or lower crustal source rocks (Collins and others, 1982; Clemens and others, 1986; Patiňo Douce, 1997); (4) melting of mantle-derived underplated basalts (for example Jahn and others, 2009); and (5) metasomatism of granitic magmas (Taylor and others, 1981). In order to contribute to the debate over the origin of the A-type granitoids in the CAOB and elsewhere, we present data on petrography, mineral chemistry, geochronology and geochemistry including major and trace elements and Nd and Sr isotopic ratios for the rocks of the Dashibalbar pluton (central Mongolia) and related units and discuss their petrogenetic significance as well as the tectonic setting.

GEOLOGICAL SETTING

The Early Mesozoic, North-Gobi rift is characterized by Triassic, bimodal volcanic suites intruded by alkaline granites (figs. 1 and 2). The North-Gobi rift forms one of a series of Permian-Early Cretaceous rift belts that curve around the southern margin of

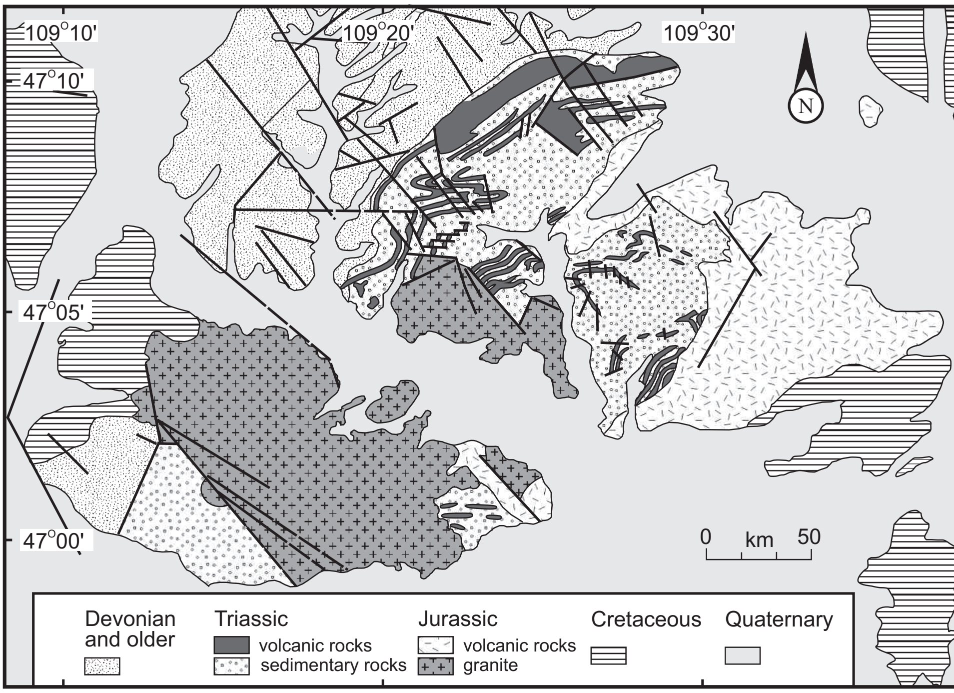

Fig. 3. Geological map of the Dashibalbar igneous complex (modified after Kalimulin, 1968).

the Siberian craton (Yarmolyuk and Kuzmin, 2011). These belts formed after amalgamation of the CAOB during the Paleozoic orogenies (Jahn and others, 2009). The North-Gobi rift occurs in the central part of the CAOB and is bounded to the west by the Kharkhorin (Karakorum) rift that is intruded by the Khentey batholith and by the Western Trans-Baikalian rift near the northern margin of the CAOB (figs. 1 and 2). The rifts are filled by Upper Triassic clastic sedimentary rocks, overlain by bimodal volcanic suites composed of basalts and rhyolites or comendites (Yarmolyuk and others, 2002). These Early Mesozoic units were intruded by granitic plutons. Both the volcanic complexes and granitic plutons form relatively small, isolated, but numerous bodies, typically preserved only in the rifts. The size of the plutons ranges from tens to several hundred km^2. The rifts are locally overlain by Early Cretaceous basaltic rocks and sedimentary rocks, commonly deposited within still younger rift structures with similar regional trends.

The Dashibalbar pluton (fig. 3), located about 300 km east of Ulaanbaatar, is one of many granitoid intrusions in the rift system. The Dashibalbar part of the North-Gobi rift is a NE-trending rift filled with the Upper Triassic, fossiliferous gray terrigenous sediments that are interbedded in the upper part with silicic volcanic rocks. The sedimentary strata are up to 2,000 m thick in the central part of rift; they were gently folded prior to the emplacement of the Early Jurassic bimodal volcanic suite and the intrusion of the Dashibalbar pluton. The Triassic strata unconformably overlie fossiliferous Lower to Middle Devonian sedimentary sequences (Kalimulin, 1968).

The Dashibalbar pluton (~300 km^2), which intruded the Triassic sedimentary rocks and the bimodal volcanic suite (Yarmolyuk and others, 2002), has a roughly rectangular shape, and is bounded by NW-trending faults that are approximately perpendicular to the rift (fig. 3). One of these faults not only offsets contacts with its host rocks but also divides the pluton into two parts (fig. 3). The eastern margin of the pluton is in fault contact with the Early Jurassic bimodal volcanic suite composed of basalts and comendites/rhyolites (fig. 3). The northeastern part of the pluton probably represents an apical segment of the intrusion. The pluton is cut by numerous granitic, quartz syenitic and aplitic dikes. The dikes typically trend E to SE, are ~1 to 20 m wide, and, based on their mineralogy and geochemistry, are assumed to be related to the complex. The granite contains enclaves of host sedimentary rocks (siltstone and sandstone) as well as syenitic rocks. The syenitic enclaves are typically rounded, ≤50 cm in diameter, and have the sharp contacts. Locally, they constitute about 5 volume percent of the outcrops whereas elsewhere they are absent. The association of granitic intrusions with the bimodal volcanic complexes is common in this part of the CAOB.

ANALYTICAL METHODS

A 3 kg sample of amphibole granite from the pluton was collected for U-Pb zircon dating by laser ablation inductively-coupled plasma mass spectrometry (LA-ICP-MS). Zircons were separated by conventional magnetic and heavy liquid technique and subsequently mounted to perform cathode-luminescence and backscatter imaging. The U, Th and Pb isotopic analyses were performed on 120 zircon grains (Appendix 1) at the Geochronology lab of the Senckenberg Naturhistorische Sammlungen Dresden, Museum fur Mineralogie und Geologie (Germany) using a Thermo-Scientific Element 2XR sector field ICP-MS coupled to a New Wave UP-193 Excimer Laser System (Appendix 1). A detailed description of the analytical procedure is given by Hofmann and others (2011). A Concordia diagram (2 sigma error ellipses) and Concordia ages (95% confidence level) were generated using Isoplot/Ex 2.49 (Ludwig, 2001) and the Age Display program (Sircombe, 2004) was used to produce frequency and relative probability plots.

Mineral compositions were determined using (1) a JEOL 8200 electron microprobe equipped with four wavelength-dispersive spectrometers (WDS) and one energy dispersive spectrometer (EDS), and (2) a LEO 1450VP scanning electron microscope (SEM) equipped with an Oxford INCA X-max 80 mm^2 SDD EDS detector. The microprobe (WDS) was employed to determine the compositions of ferromagnesian minerals (table 1) whereas the SEM was used to determine the composition of feldspars (table 2). The analyses of accessory minerals were done using both instruments. Recent work (Ritchie and others, 2012; Owen, 2012) has shown that microprobe WDS data can be reproduced by SEM EDS.

Whole rock major and trace elements (table 3; Appendix 2) were determined using lithium tetraborate fusion at the Activation Laboratories, Ancaster, Ontario, Canada. Major elements and some trace elements (V, Ni, Zn, Rb, Ba, Sr, Y, Ga, Nb, La, Ce and Zr) were determined in 39 samples by inductively coupled plasma-optical emission spectrometry, whereas other trace elements (REE, Th, U, Ta, Nb and Hf) were analyzed in 28 of these samples using a Perkin Elmer Optima 3000 inductively coupled plasma mass spectrometer. Based on replicate analyses, the precision is generally between 2 and 10 percent for trace elements and 3 to 5 percent for major elements.

Ten samples were analyzed for Sr and Nd isotopic ratios at the Institute of Earth Sciences, Academia Sinica, Taipei. The chemical separation and isotopic measurements are described in Shellnutt and others (2012). $^{143}Nd/^{144}Nd$ ratios were normalized to $^{146}Nd/^{144}Nd=0.7219$ and $^{87}Sr/^{86}Sr$ ratios to $^{86}Sr/^{88}Sr=0.1194$. The Sr isotope ratios were measured using a Finnigan MAT-262 thermalionization mass spectrometer (TIMS), whereas the Nd isotope ratios were measured using a Finnigan Triton TIMS. The 2 σ values for all samples are less than or equal to 0.000020 for $^{87}Sr/^{86}Sr$ and less than or equal to 0.000008 for $^{143}Nd/^{144}Nd$ (table 4). The measured isotope ratios for

Table 1

Compositions of ferromagnesian minerals in representative samples of granitoid rocks

	syenite			granite															
Sample #	DB-26C			DB-39				DB-4	DB-25		DB-28		DB-33		DB-35	DB-37		DB-41	
		Ferro-richterite*		Cpx		F-ferro-richterite		F-ferro-richterite	kataphorite		F-ferrorichterite		F-ferrorichterite		F-ferro-richterite**	F-ferrorichterite		F-ferrorichterite	
	Cpx		Bt	core	rim		Bt		core	rim	core	rim	core	rim		core	rim	core***	rim****
SiO_2 (%)	55.81	54.85	40.21	52.72	52.24	46.92	38.41	48.19	48.91	49.5	47.27	48.18	47.86	49.93	47.52	47.97	50.39	47.03	50.01
TiO_2		0.80	5.245			0.48	2.85	1.40	1.42	0.84	0.19	0.26	0.86	0.33	0.31	1.45	1.36	1.66	1.33
Al_2O_3		1.95	14.01	0.43	0.33	3.11	9.30	1.75	3.89	3.31	3.40	2.11	1.92	1.34	2.32	2.57	3.03	2.58	2.14
FeO	17.73	20.83	23.03	13.67	14.4	23.18	28.30	30.19	25.72	25.6	30.52	32.18	31.84	34.51	31.78	31.34	31.36	30.05	29.13
MnO	0.63	0.58	0.305	0.39	0.27	0.52	0.33	0.88	0.89	0.77	0.62	0.70	0.90	0.73	0.64	0.80	0.91	0.74	0.81
MgO	5.92	7.93	5.605	12.5	11.51	5.79	6.44	2.29	5.62	6.18	2.52	1.54	1.85	0.48	1.38	1.66	1.69	2.14	2.68
CaO	17.62	6.95		18.7	20.89	5.98	0.00	5.99	8.06	8.37	7.43	6.15	5.85	3.25	5.88	4.98	6.10	6.24	5.19
Na_2O	2.28	4.77	0.305	0.31	0.19	4.01	0.01	4.87	4.25	4.27	4.32	4.19	4.89	6.76	4.43	4.75	4.88	4.81	6.51
K_2O		1.19	9.28	0.01		1.04	9.39	1.11	1.24	1.14	0.96	1.07	1.00	0.91	1.03	1.07	1.04	1.27	1.02
F						1.02	1.48	0.84			0.84	0.65	0.71	0.66	0.78	0.34	0.79	0.72	1.32
SUM	99.99	99.85	97.99	98.73	99.83	92.06	96.51	97.52	100.00	99.99	98.07	97.02	97.68	98.89	96.08	96.93	101.52	97.24	100.13
# oxygens	6	23	11	6	6	23	11	23	23	23	23	23	23	23	23	23	23	23	23
Si	2.134	7.554	3.005	2.016	1.996	7.713	2.98	7.505	7.428	7.29	7.46	7.77	7.618	7.804	7.732	7.685	7.716	7.505	7.641
Ti		0.090	0.295			0.059	0.166	0.199	0.095	0.12	0.023	0.032	0.103	0.039	0.038	0.175	0.157	0.199	0.153
Al		0.342	1.234	0.019	0.015	0.603	0.851	0.485	0.585	0.77	0.632	0.401	0.36	0.247	0.445	0.485	0.547	0.485	0.385
Fe^{3+}						0.147		0.604	0.622	0.62	0.737	0.32	0.715	1.126	0.427	0.282	0.168	0.604	0.95
Fe^{2+}	0.567	2.596	1.439	0.459	0.46	3.04	1.836	3.406	2.588	2.51	3.292	4.02	3.524	3.385	3.897	3.917	3.848	3.406	2.773
Mn	0.02	0.073	0.02	0.013	0.009	0.072	0.022	0.1	0.098	0.09	0.083	0.096	0.121	0.097	0.088	0.109	0.118	0.1	0.105
Mg	0.337	1.762	0.625	0.712	0.655	1.419	0.745	0.509	1.382	1.52	0.593	0.37	0.439	0.112	0.335	0.396	0.386	0.509	0.61
Ca	0.722	1.11		0.766	0.855	1.053		1.067	1.345	1.29	1.256	1.063	0.998	0.544	1.025	0.855	1.001	1.067	0.85
Na	0.169	1.378	0.045	0.023	0.014	1.278	0.002	1.488	1.242	1.2	1.322	1.31	1.509	2.049	1.398	1.475	1.449	1.488	1.929
K		0.226	0.885			0.218	0.929	0.259	0.218	0.15	0.193	0.22	0.203	0.181	0.214	0.219	0.203	0.259	0.199
F						0.53	0.363	0.363			0.419	0.332	0.357	0.326	0.401	0.172	0.383	0.363	0.638
X_{mg}	0.37	0.40	0.30	0.61	0.59	0.32	0.29	0.13	0.35	0.38	0.15	0.08	0.11	0.03	0.08	0.09	0.09	0.13	0.18

Amphibole analyses were recalculated using WinAmphcal software (Yavuz, 2007) and the 16CAT normilization scheme that has been shown to provide comparable estimates of the site occupancies of the various cations as wet-chemical data (Robinson and others, 1982). The average (of calculated minimum and maximum values) oxidation ratio ($Fe^{3+}/(Fe^{3+} + Fe^{2+})$) for each analysis is reported here. Using the 16CAT scheme, the T, C, and B sites are generally full or have small deficiencies. A-site occupancy exceeds 0.6 ions *pfu* based on 23 oxygen unit cell. Bt—biotite; Cpx—clinopyroxene; *partly replaces Cpx; **fibrous; ***fluorian potassic ferrorichterite; ****ferrian fluorian ferrorichterite.

Table 2

Composition of zoned plagioclase inclusions in perthite in a syenite enclave

	Zoned plg.* in perthite	Perthite* host	Perthite* host	Whole plg. grain	Perthite* host	Zoned plagioclase Core					Rim
SiO_2 (%)	63.3	67.09	67.71	62.49	66.79	59.01	60.67	64.13	65.74	65.94	65.69
Al_2O_3	22.49	18.08	18.10	24.18	19.14	26.83	25.75	23.25	21.6	21.32	20.99
FeO	0.57	0.67	0.30		0.46						
CaO	3.19	0.41		2.86	0.70	4.41	4.94	2.30	0.78		0.60
Na_2O	10.19	7.82	7.58	9.72	9.32	9.76	8.65	10.32	11.07	9.32	12.06
K_2O	0.26	5.94	6.31	0.75	3.58				0.8	3.42	0.66
SUM	100.00	100.01	100.00	100.00	99.99	100.01	100.01	100.00	99.99	100.00	100.00
# oxygens	8	8	8	8	8	8	8	8	8	8	8
Si	2.808	3.006	3.025	2.766	2.97	2.628	2.688	2.821	2.984	2.988	2.899
Al	1.176	0.955	0.953	1.262	1.004	1.409	1.345	1.206	1.121	1.112	1.092
Fe	0.21	0.025	0.011		0.017						
Ca	0.152	0.02		0.136	0.033	0.21	0.235	0.108	0.037		0.028
Na	0.877	0.679	0.657	0.834	0.804	0.843	0.743	0.88	0.945	0.8	1.032
K	0.003	0.34	0.36	0.042	0.203				0.045	0.193	0.037
X_{An}	0.145	0.019		0.134	0.032	0.199	0.24	0.109	0.036		0.026
X_{Ab}	0.841	0.654	0.646	0.824	0.773	0.801	0.76	0.891	0.920	0.806	0.940
X_{Or}	0.014	0.327	0.354	0.042	0.195				0.044	0.194	0.034

plg—plagioclase; *whole grain (reintegrated).

JMC Nd standard is 0.511813 ± 0.000010 (2σ) and NBS987 Sr standard is 0.710248±0.00001 (2σ). The initial $^{87}Sr/^{86}Sr$ isotopic ratios as well as $\varepsilon_{Nd(t)}$ were calculated using the age of 186 Ma.

Petrography and Mineral Chemistry

The Dashibalbar pluton consists predominantly of medium-grained (on average, ~5-10 mm), locally K-feldspar-phyric, amphibole-bearing, alkali feldspar granite. It contains enclaves of mineralogically-similar syenitic rocks, and is cut by quartz alkali feldspar syenite dikes.

The granitic (*sensu lato*) rocks of the Dashibalbar pluton are dominated by xenomorphic to subidiomorphic perthite, with interstitial quartz, and well-formed ([sub]idiomorphic) amphibole (~5 vol.%) that commonly encloses perthite crystals. Biotite and/or rare pyroxene occur in a few samples. The pyroxene is partly resorbed by amphibole, whereas the amphibole typically is partly mantled by biotite. Accessory minerals include zircon and fluorapatite; some samples also contain various combinations of magnetite, ilmenite, Ce-monazite, and/or fluorite.

The dike rocks are equigranular to K-feldspar (perthite)-phyric. Like the rocks they cut, they are dominated by perthite and contain subordinate, interstitial quartz, but myrmekite and cuneiform (graphic) textures are conspicuous, and their ferromagnesian minerals are altered to Fe oxides ± actinolite, a feature not seen in their host rocks.

The granitoid enclaves are (quartz) syenitic and typically porphyritic and finer grained than the host rock. The microgranitoid enclaves have sharp contacts with the

Table 3

Major and trace element composition of the rocks of the Dashibalbar complex

	Granite						Dike			
Sample	DB-2	DB-6	DB-11	DB-20D	DB-28	DB-40	DB-13	DB-15	DB-15A	DB-16
SiO_2 (%)	76.29	72.81	75.04	75.21	74.04	74.37	70.92	67.17	68.02	69.34
TiO_2	0.20	0.27	0.15	0.19	0.27	0.27	0.24	0.47	0.44	0.36
Al_2O_3	11.79	12.86	13.16	12.84	12.65	12.61	14.23	14.92	14.15	14.31
$Fe_2O_3^*$	2.71	3.00	2.35	2.52	3.05	2.71	3.59	6.11	5.69	4.43
MnO	0.01	0.07	0.03	0.03	0.06	0.05	0.08	0.13	0.13	0.10
MgO	0.00	0.08	0.10	0.07	0.10	0.08	0.05	0.23	0.17	0.12
CaO	0.07	0.45	0.20	0.35	0.49	0.39	0.42	0.40	1.13	0.67
Na_2O	4.34	4.35	4.49	3.94	4.32	4.30	4.38	4.51	4.31	4.49
K_2O	4.33	4.78	3.68	4.24	4.51	4.62	4.79	4.50	4.80	4.54
P_2O_5	0.07	0.05	0.02	0.03	0.04	0.05	0.03	0.09	0.08	0.07
LOI	0.19	0.40	0.39	0.69	0.15	0.19	0.70	0.87	0.89	1.07
SUM	100.00	99.12	99.61	100.10	99.67	99.63	99.43	99.40	99.80	99.49
Cr (ppm)	0	0	0	0	0	0	0	0	0	0
Ni	4	3	4	3	3	3	5	4	3	3
V	7	10	9	11	11	11	7	11	11	11
Zn	83	129	92	145	118	131	134	138	124	120
Rb	133	163	85	182	160	161	143	149	143	132
Ba	55	152	379	132	135	137	837	1377	1761	1635
Sr	10	21	63	28	24	23	37	77	101	54
Ga	29	26	23	30	26	26	26	27	24	25
Ta	1.5	1.8	1.7	2.2	1.4	1.5	1.4	1.4	1.4	1.8
Nb	27.6	32.3	23.5	30.7	31.6	30.0	23.5	24.9	24.5	22.7
Hf	18.3	20.1	12.9	20.8	20.0	18.7	16.4	19.5	18.4	15.9
Zr	688	734	441	761	779	661	624	918	860	624
Y	76	81	67	93	71	58	67	72	56	69
Th	16.7	17.9	15.4	22.9	16.8	17.3	14.9	12.3	11.7	14.1
U	4.1	2.9	4.4	10.8	3.4	3.3	4.2	3.7	3.3	4.9
La	46.7	86.4	68.6	66.0	52.3	61.7	61.7	67.4	43.2	61.0
Ce	125.3	186.0	152.0	142.0	173.7	154.1	142.5	147.2	109.6	134.8
Pr	12.95	22.18	18.17	18.76	15.38	16.87	17.09	18.44	12.97	16.55
Nd	50.5	84.6	73.6	75.5	59.6	64.5	71.5	73.4	54.6	69.0
Sm	10.41	16.27	13.65	16.08	12.04	12.40	13.36	15.32	11.34	13.85
Eu	0.62	0.43	1.03	0.68	0.34	0.34	1.68	3.27	2.77	2.46
Gd	10.58	14.63	12.64	14.63	11.19	9.97	11.94	13.26	9.61	12.29
Tb	1.96	2.50	2.06	2.59	1.99	1.80	2.00	2.23	1.62	2.09
Dy	12.93	15.04	12.71	16.63	12.51	11.39	12.57	13.09	10.18	12.77
Ho	2.79	2.98	2.53	3.24	2.63	2.17	2.33	2.62	1.96	2.50
Er	8.30	8.97	7.41	9.53	7.90	7.16	7.00	7.61	5.80	7.42
Tm	1.28	1.37	1.14	1.50	1.29	1.10	1.08	1.22	0.92	1.12
Yb	8.61	9.38	7.45	9.84	9.07	7.94	7.31	7.83	6.70	7.44
Lu	1.30	1.33	1.09	1.41	1.26	1.17	1.04	1.18	0.95	1.08
A/NK	1.00	1.04	1.16	1.16	1.06	1.09	1.15	1.21	1.15	1.16
A/CNK	0.99	0.98	1.12	1.10	0.98	0.99	1.08	1.15	0.99	1.06
Eu/Eu*	0.18	0.09	0.24	0.14	0.09	0.09	0.41	0.70	0.81	0.58
$(La/Yb)_n$	3.63	6.16	6.16	4.49	3.86	5.20	5.69	5.76	9.31	5.48

TABLE 3
(continued)

	Syenite				Rhyolite	Basalt
Sample	DB-26	DB-26B	DB-27	DB-34	DB-22	DB-21
SiO_2 (%)	68.32	63.36	66.31	63.84	72.39	50.75
TiO_2	0.51	0.76	0.56	0.88	0.34	2.03
Al_2O_3	14.34	16.09	16.12	16.64	12.54	15.90
$Fe_2O_3^*$	3.63	4.61	3.93	3.81	4.40	11.49
MnO	0.08	0.14	0.08	0.07	0.09	0.20
MgO	0.38	0.80	0.51	0.71	0.00	4.78
CaO	1.10	1.68	1.11	1.46	0.98	7.10
Na_2O	5.02	5.87	5.57	5.83	3.59	4.53
K_2O	5.45	5.80	5.62	5.41	5.72	1.58
P_2O_5	0.14	0.25	0.13	0.28	0.02	0.35
LOI	0.67	0.40	0.29	0.40	0.00	1.69
SUM	99.64	99.76	100.23	99.33	100.07	100.40
Cr (ppm)	0	0	0	0	0	97
Ni	5	7	5	4	3	18
V	45	35	21	24	9	218
Zn	184	124	119	183	92	139
Rb	138	142	218	320	126	54
Ba	646	555	478	189	61	437
Sr	162	131	90	32	51	476
Ga	25	25	27	24	25	20
Ta	1.0	0.8	1.5	2.1	1.6	0.9
Nb	22.3	21.4	38.9	39.0	29.9	12.3
Hf	18.8	19.9	17.8	17.5	22.5	5.7
Zr	914	867	756	667	859	220
Y	71	77	100	81	74	36
Th	8.4	7.6	9.2	14.4	19.5	3.1
U	5.5	2.0	1.6	7.8	5.4	0.7
La	84.0	79.5	80.8	102.9	70.4	22.3
Ce	140.5	155.9	129.8	235.0	155.8	53.4
Pr	24.70	20.55	20.84	31.13	18.43	7.18
Nd	98.1	82.6	92.3	127.8	71.3	33.0
Sm	18.06	15.17	18.74	25.28	14.06	7.21
Eu	1.74	1.55	1.19	0.60	0.58	2.24
Gd	15.05	15.02	20.45	19.29	12.68	7.39
Tb	2.35	2.43	3.17	2.99	2.15	1.19
Dy	13.53	15.15	19.15	16.43	14.12	6.73
Ho	2.51	2.97	3.47	2.91	2.77	1.33
Er	7.15	8.52	9.94	8.81	8.64	3.72
Tm	0.97	1.28	1.36	1.39	1.27	0.55
Yb	6.51	8.32	8.89	9.19	8.56	3.70
Lu	0.87	1.11	1.20	1.40	1.26	0.52
A/NK	1.01	1.01	1.06	1.08	1.04	1.74
A/CNK	0.89	0.85	0.93	0.92	0.90	0.72
Eu/Eu*	0.32	0.31	0.19	0.08	0.13	0.94
$(La/Yb)_n$	8.63	6.39	6.08	7.49	5.50	4.03

Fe_2O_3* = total Fe as Fe_2O_3; A/NK = $Al_2O_3/(Na_2O + K_2O)$ (mol%); A/CNK = $Al_2O_3/(CaO + Na_2O + K_2O)$ (mol%).

TABLE 4

Whole rock Sr and Nd isotopic data for the Dashibalbar complex

Sample	Rock	Rb (ppm)	Sr (ppm)	$^{87}Rb/^{86}Sr$	$^{87}Sr/^{86}Sr$	± $2s_m$	$^{87}Sr/^{86}Sr_i$ (186 Ma)	Sm (ppm)	Nd (ppm)	$^{147}Sm/^{144}Nd$	$^{143}Nd/^{144}Nd$	± $2s_m$	$\varepsilon_{Nd(0)}$	$\varepsilon_{Nd(t)}$ (186 Ma)	T_{DM} (Ma)
DB-6	Granite	163	24	19.7	0.758089	7	0.705861	16.27	84.6	0.1163	0.512585	6	-1.0	0.9	884
DB-11	Granite	84	63	3.8	0.716013	7	0.705802	13.65	73.6	0.1121	0.512582	7	-1.1	0.9	853
DB-28	Granite	163	22	21.6	0.761664	9	0.704669	12.04	59.6	0.1221	0.512611	6	-0.5	1.2	897
DB-15	Dike	154	73	6.1	0.723218	7	0.707050	15.32	73.4	0.1262	0.512591	7	-0.9	0.8	974
DB-16	Dike	133	51	7.6	0.726386	6	0.706394	13.85	69	0.1214	0.51259	7	-0.9	0.9	924
DB-26B	Syenite	149	131	3.3	0.714442	8	0.705733	15.17	82.6	0.1110	0.512616	6	-0.4	1.6	793
DB-27	Syenite	226	90	7.3	0.725833	7	0.706583	18.74	92.3	0.1227	0.512622	6	-0.3	1.4	885
DB-34	Syenite	320	30	31.1	0.788009	10	0.705749	25.58	127.8	0.1210	0.512614	6	-0.5	1.3	882
DB-22	Rhyolite	131	51	7.4	0.726155	8	0.706464	14.06	71.3	0.1192	0.512671	7	0.6	2.5	773
DB-21	Basalt	55	476	0.33	0.706005	7	0.705121	7.21	33	0.1321	0.512699	6	1.2	2.7	843

(1) Rb, Sr, Sm and Nd concentrations were obtained by ICP-MS and have precision less than ±2%.
(2) The results of isotopic measurements for Sr and Nd reference materials are: NBS-987 (Sr) = 0.710248 ± 3 ($2s_m$). JMC (Nd) = 0.511813 ± 10 ($2s_m$).
(3) T_{DM}-Nd model ages were calculated based upon a depleted mantle model separated from the CHUR (chondrite-uniform resevoir) at 4.55 Ga, with linear evolution and a present-day epsilon value of +10.
(4) $^{87}Sr/^{86}Sr_i$ (186 Ma) and $\varepsilon_{Nd(t)}$ (186 Ma)—age corrected to 186 Ma.

host rock, and lack lobate margins indicative of magma mingling. They contain various combinations of amphibole, perthite and rare clinopyroxene phenocrysts (to 5 mm) set in a fine-grained (~0.1-0.3 mm), perthite-rich groundmass that contains interstitial quartz. Some enclaves contain small amounts (~1 vol.%) of plagioclase mantled by perthite. Amphibole phenocrysts can be poikilitic, enclosing well-formed (idiomorphic) perthite oikocrysts. In some enclaves, biotite is spatially associated with amphibole. Zircon and apatite are conspicuous accessory phases.

Most samples of granites and syenites from the Dashibalbar pluton contain Ca-Na amphibole. The amphiboles form xenomorphic to subidiomorphic crystals up to 2 mm in diameter and generally occur in clusters. Based on the recent IMA-approved classification scheme for the amphiboles (compare Hawthorne and Oberti, 2007), the Ca-Na amphiboles in granitoid rocks of the Dashibalbar pluton correspond to fluorian ferrorichterites with 0.3 to 1.2 weight percent F and X_{mg} (=Mg/Mg+Fe) ratios < 0.2, whereas F-free amphiboles are richterites and katophorites with relatively high X_{mg} ratios (0.23-0.62) (table 1). The low X_{mg} values of F-bearing amphiboles point to the enrichment of F in the residual, fractionated magma. The relatively magnesian amphiboles can be partly enclosed by matrix perthite, closely resembling subophitic texture. In some instances, these amphibole grains partly replace early pyroxene.

Primary biotite occurs as subidiomorphic grains up to 1 mm in diameter that commonly have nucleated on clusters of amphibole crystals. They have X_{mg} ratios between 0.27 and 0.30 and contain 2.7 to 3.3 weight percent TiO_2. Secondary biotite is nearly pure annite (X_{mg} = 0.02) notwithstanding similar titania contents as the primary biotite. The ferromagnesian minerals are set in a perthitic matrix. The perthite consists of microcline ($Or_{98}Ab_2$) that has exsolved nearly pure albite. The reintegrated composition of perthite varies between $Ab_{33}Or_{66}$ and $Ab_{77}Or_{20}$. In some syenitic enclaves, perthite encloses normally-zoned oligoclase (An_{24} to An_{14}; table 2) that is mantled by albite (An_4).

Rare augite ($X_{mg} \sim 0.6$) in granites contains negligible non-quadrilateral components (Ti = 0, Al = 0.018 ions *pfu,* Na = 0.02 ions *pfu,* calculated $Fe^{3+} = 0$ [per Droop, 1987]). The pyroxene coexists with fluorian ferrorichterite (table 1). Aegirine was not detected in any of the granitoid rocks. Relict calcic pyroxene in syenitic xenoliths is relatively iron-rich (X_{mg} = 0.38). It is largely replaced by F-free Ca-Na amphibole. Accessory minerals include various combinations of zircon, fluorapatite, magnetite, ilmenite, zircon, Ce-monazite, and/or fluorite. Zircon contains up to 2.5 weight percent HfO_2. Magnetite contains up to ~10 weight percent TiO_2. The MnO content of ilmenite averages ~2.5 weight percent. The Ce-monazite contains 28 to 32 weight percent Ce_2O_3, 6 to 8 weight percent Nd_2O_3, and 13 to 17 weight percent La_2O_3.

The basalts of the underlying volcanic complex are porphyritic with clinopyroxene phenocrysts set in fine grained matrix. The phenocrysts typically are large (to 5 mm), fresh augite crystals ($En_{43}Fs_{17}Wo_{40}$) with low (<0.5 wt. %) contents of TiO_2 and Na_2O. Matrix plagioclase is completely saussuritized. Accessory minerals include ilmentite, magnetite, zircon, baddeleyite (enclosed by zircon), apatite, Ce-monazite, a Nd-bearing Ti-Fe-Ce-rich silicate apparently belonging to the chevkinite group of minerals, and a Cu-rich alloy. The base metal alloy is dominated by Cu (60-100%), but can contain 20 to 35 weight percent Zn, and up to 5 weight percent Pb. It appears to be a metallic alloy, and not an oxide phase.

The rhyolites/comendites of the volcanic complex are extremely fine grained (essentially glassy), and exhibits flow banding on a 0.1 to 5 mm scale. They contain idiomorphic K-feldspar and rounded and embayed quartz phenocrysts. Accessory minerals include magnetite and traces of Ce-monazite and a chevkinite-like mineral with about 16 weight percent Ce_2O_3 and 20 weight percent TiO_2, but which has much lower Nd_2O_3 (4 wt. %) and higher silica (34 wt. %) than *bona fide* Ce-chevkinite.

GEOCHRONOLOGY

Zircons (119 grains) from amphibole-bearing granite give a Concordia U-Pb zircon age of 186 ± 1 Ma (weighted mean; two-sigma; fig. 4; Appendix 1), which is interpreted as the time of crystallization of the intrusion. There is also an analysis of zircon with an age of about 400 Ma that is inferred to represent an inherited age. The inheritance age is probably a result of crustal contamination of the granitic magma by Devonian basement. The 186 Ma age is within error of the $^{40}Ar/^{39}Ar$ amphibole age of the Dashibalbar granites reported by Yarmolyuk and others (2002) who obtained an age of 188.7 ± 2.8 Ma. Yarmolyuk and others (2002) also dated comendites from the bimodal volcanic suite intruded by the pluton. Their whole-rock Rb-Sr dating gave an age of 195.9±3.9 Ma, implying a time gap between the emplacement of volcanic complex and the intrusion.

The U-Pb zircon age falls between two alkaline granitoid magmatic stages reported from the Mongolian-Transbaikalian igneous province by Jahn and others (2009): Late Triassic (230-190) and Late Jurassic-Early Cretaceous (~150-120 Ma) suggesting a migration and/or continuity of magmatic activities in the central Mongolian part of the CAOB.

GEOCHEMISTRY

Granitic Intrusion

Major elements.—The granites (table 3) have high SiO_2 (68-78 wt.%) and Na_2O+K_2O (~7.5-9.5 wt.%) contents with $Na_2O/K_2O \sim 0.6–1$ but are low in CaO (<0.6 wt.%) and MgO (~0.1 wt.%). According to the alkali-silica diagram (fig. 5), most rocks correspond to alkaline granites. On De la Roche and others' (1980) multicationic diagram (fig. 6), the rocks plot into the field of alkaline granites. The A/CNK (molar $Al_2O_3/CaO+Na_2O+K_2O$) values vary mostly from 0.95 to 1.2 (fig. 7). The agpaitic index [A/NK (molar Al_2O_3/Na_2O+K_2O)] of the granites ranges typically from 1 to 1.2, implying that most of them are peraluminous or metaluminous (fig. 7). However, according to the classification scheme of Liegeois and others (1998), most of these rocks are alkaline (A/NK<1.15). Several features of the major element chemistry such as low Al_2O_3, CaO and MgO are typical of A-type granites (Whalen and others, 1987; Eby, 1992). The granites have high $Fe_2O_{3(total)}/(Fe_2O_{3(total)}+MgO)$ ratio due to elevated Fe contents ($Fe_2O_3 \sim$ 2-6 wt.%) and are typical ferroan (A-type) granite of Frost and others (2001). The major element composition of dikes is similar to that of the granites (figs. 5 and 6) although the dikes contain less silica and are less evolved. The compositional characteristics are consistent with a genetic relationship between the spatially associated granites and dikes (figs. 5 and 6).

Compared to the granites, the enclaves have a lower SiO_2 content (63-68 wt. %). This is also shown on the De la Roche and others' (1980) classification diagram (fig. 6) where the enclaves are quartz syenites and syenites. The syenites are still quartz normative (>1 % normative quartz). The Na_2O/K_2O ratio of the enclaves is ~1 with the total alkalis ~10.5 to 12 weight percent (fig. 5). The syenites have higher alkalis, TiO_2 (0.5-0.9 wt.%), Al_2O_3 (14.5-17 wt.%), $Fe_2O_{3\ (tot)}$ (4-5 wt.%), MgO (0.4-0.9 wt.%) and CaO (1-2 wt.%) relative to the granites.

Trace elements.—The concentrations of many lithophile trace elements including Ga, Zr, Nb and Y in the granites and dikes are high, typical of A-type granites. The A-type characteristics of the granites are also indicated by the discrimination diagram of Whalen and others (1987), which separates the A-type granites from I-, S- and M-type granites (fig. 8A). The 10,000 × Ga/Al ratio, which has been used to distinguish the A-type granites from other granitoids, ranges from ~3.4 to 4.7, values comparable to the global average of 3.75 for A-types granites (Whalen and others, 1987). Like granites and dike rocks, the enclaves are A-type rocks but have lower values of the 10,000 ×

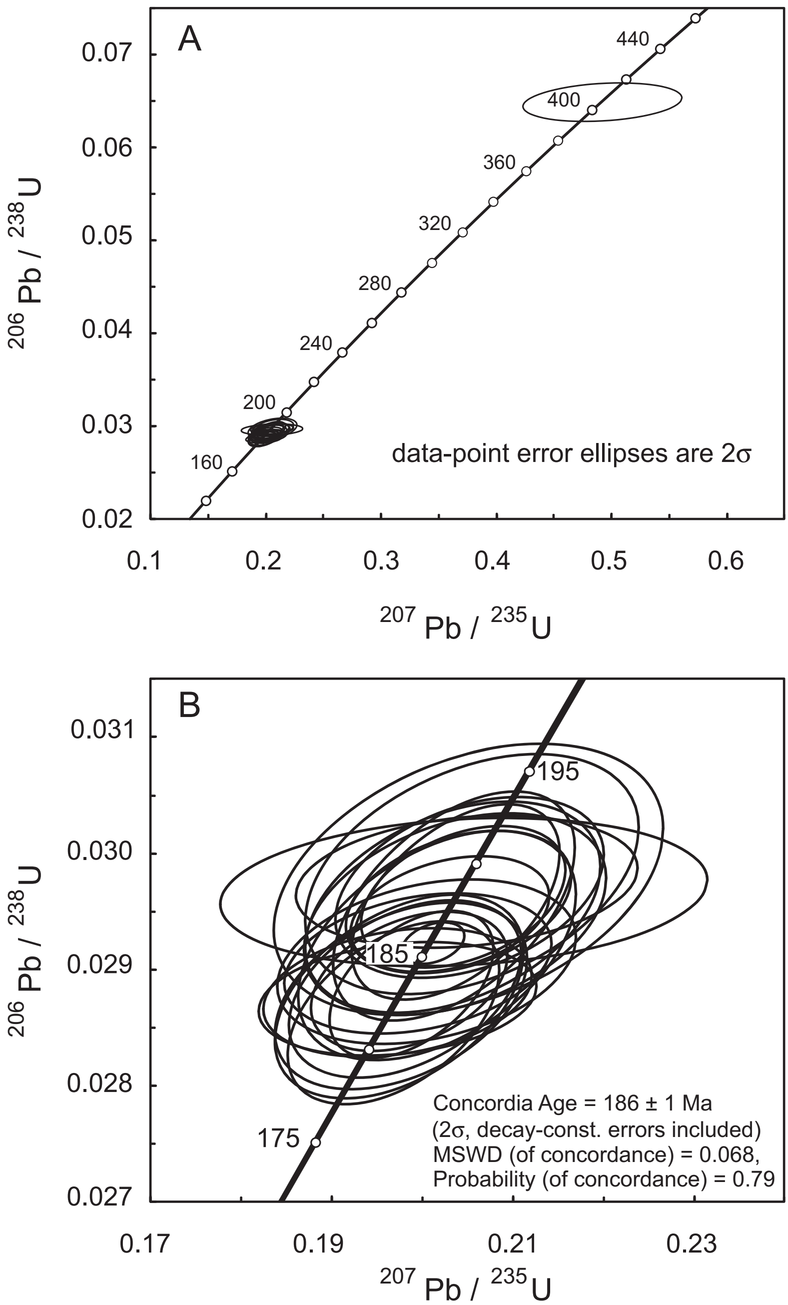

Fig. 4. Results of U-Pb zircon age dating of Mesozoic amphibole-bearing granite of the Dashibalbar pluton by LA-ICP-MS. (A) Concordia plot for the complete age (including an inherited zircon component) spectrum showing error ellipses (2 sigma); (B) enlargement of the plot; Concordia plot for the 186 Ma intrusive age showing error ellipses (2 sigma).

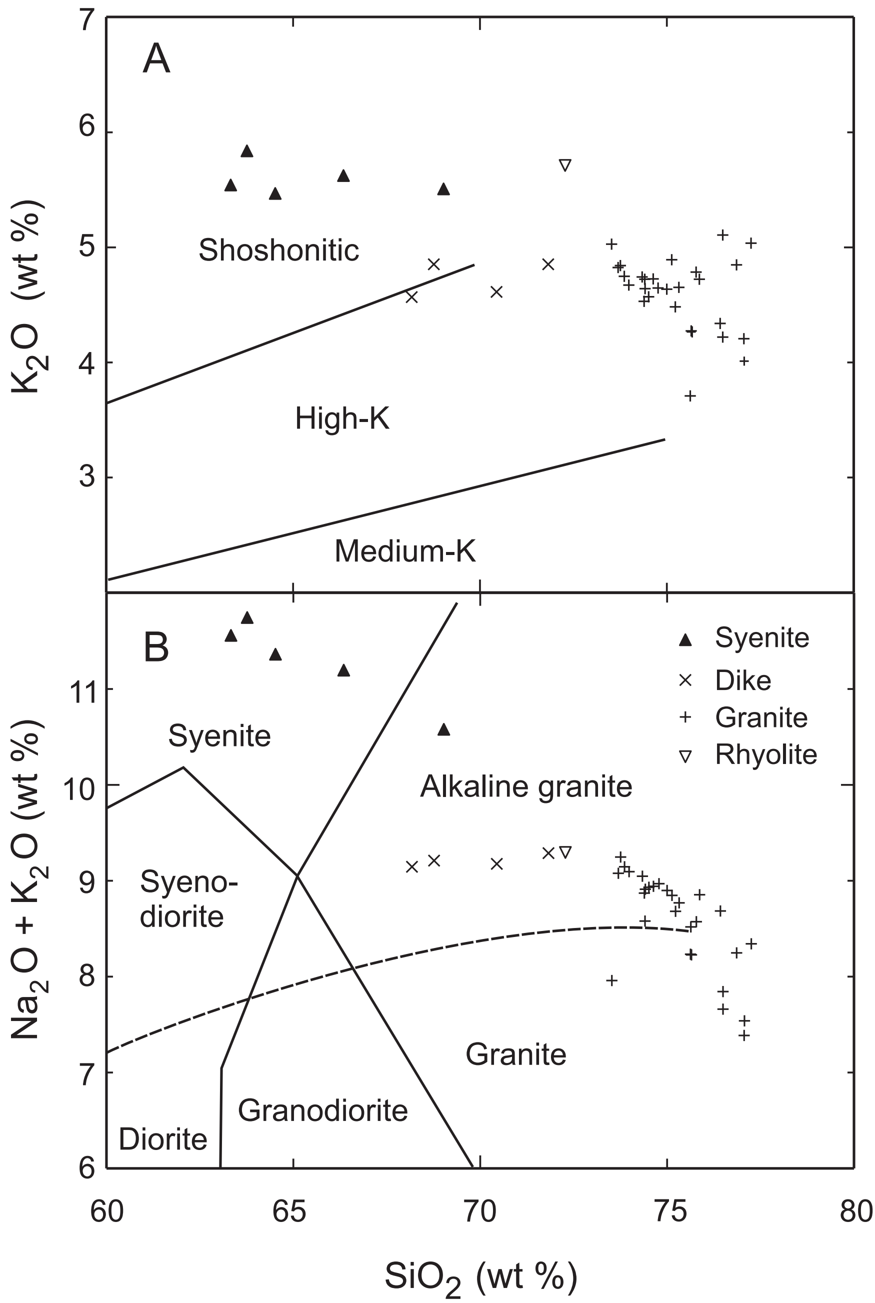

Fig. 5. Variations of SiO_2 versus K_2O and Na_2O+K_2O (wt.%) for the rocks of the Dashibalbar igneous complex. The fields in (A) are after Peccerillo and Taylor (1976), and in (B) after Cox and others (1979). Dashed line in (B) subdivides alkaline from subalkaline rocks.

Ga/Al ratio (2.7-3.3) than the granites. The enclaves are higher in Sr and Ba but have lower Rb/Sr ratios relative to the granites. Within-plate characteristics of all these rocks are also indicated by the Rb- (Nb+Y) diagram (fig. 8B) of Pearce and others (1984).

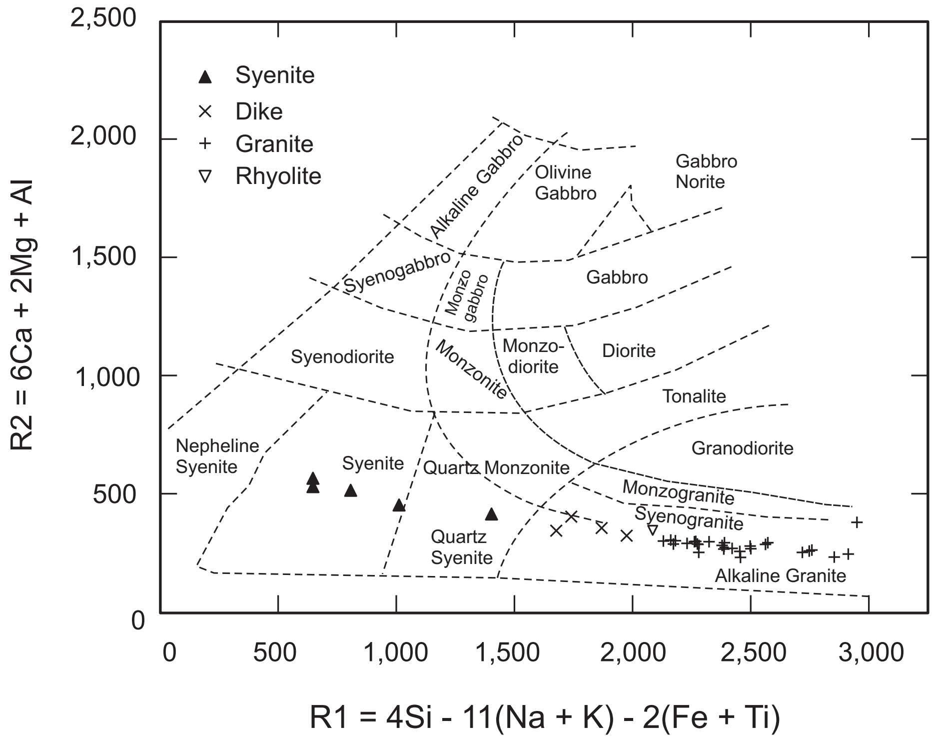

Fig. 6. The R 1 versus R 2 multicationic diagram for the rocks of the Dashibalbar igneous complex showing the empirically determined compositional fields of De la Roche and others (1980). The granites of the pluton plot into or close to the field of alkaline granites whereas the enclaves are mainly syenites.

The chondrite-normalized REE patterns (fig. 9) show that the granites are enriched in the light REE (LREE) and have unfractionated heavy REE (HREE). The $(La/Yb)_n$ values range from ~3 to 6 and $(Gd/Yb)_n$ are ~0.8 to 1.3, reflecting the nearly flat HREE segment of the patterns. All granitic samples display a distinct negative Eu anomaly with the Eu/Eu* values mostly ~0.1. The Eu/Eu* ratio shows a positive correlation with Sr and Ba, typical of feldspar fractionation. The mantle-normalized trace element plots (fig. 10) feature an enrichment in Rb, depletion of Ba and Sr as well as pronounced troughs for Ti, Eu, Nb and Ta. The negative anomalies of Sr, Ba and Eu can be attributed to feldspar fractionation whereas Fe-Ti oxide is probably responsible for Ti depletion. The flat HREE profiles indicate that garnet was not present in the source region of the granites (fig. 9).

Relative to the granites, the dikes have similar trace element distributions including the shapes of REE patterns (fig. 9) and the mantle normalized plots (fig. 10), confirming genetic relationships between these rock types. The dikes have smaller negative Eu and Ba anomalies than the granites, indicating less extensive crystallization of feldspars. In general, the dike rocks are less fractionated than the granites and probably represent a younger, less evolved pulse of magma from a similar reservoir. The enclaves have REE patterns similar to those of granites except they are slightly more fractionated with $(La/Yb)_n$ ~5.5-8 and $(Gd/Yb)_n$ ~ 1.4-1.9 but have a smaller negative Eu anomaly (Eu/Eu* ~ 0.1-0.35). These differences are also shown by their mantle-normalized patterns (fig. 10).

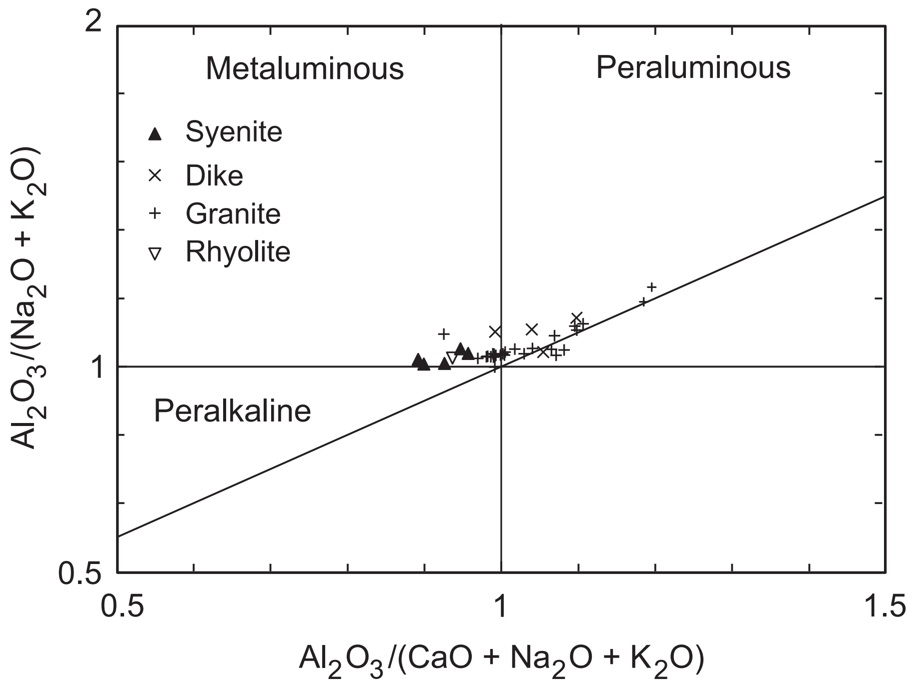

Fig. 7. Molar $Al_2O_3/(Na_2O+K_2O)$ (A/NK) versus $Al_2O_3/(CaO+Na_2O+K_2O)$ (A/CNK) diagram discriminating metaluminous, peraluminous and peralkaline compositions of granitic rocks. Most of the granitoid rocks of the Dashibalbar pluton plot into metaluminous and peraluminous fields.

Bimodal Volcanic Sequence

The slightly older bimodal volcanic suites consist of basalts and rhyolites/comendites. The basalts are subalkaline to transitional rocks with about 50 to 52 weight percent SiO_2 and Mg# (mole $Mg/Mg+Fe_{tot}$) of ~0.45 to 0.50. The fractionated character of the basalts indicated by the low Mg# is also consistent with low Cr (~100 ppm) and Ni (~20 ppm) concentrations. The basalts have high contents of TiO_2 (~2 wt.%), K_2O (~1.6 wt.%) and Zr (~220 ppm), typical of evolved tholeiitic or transitional basalts. The chondrite-normalized REE patterns of the basalts show LREE enrichment with $(La/Yb)_n$ ~ 3.5 to 4 and $(Gd/Yb)_n$ ~ 1.6 (fig. 9) and moderate absolute contents of REE including La ~ 20 to 25 ppm. Their primitive mantle-normalized pattern of incompatible elements (fig. 10) displays a gradual increase from Lu towards highly incompatible elements such as Th, accompanied by only a rather minor negative Nb anomaly. According to various discrimination diagrams (such as Cr vs Ti and Ti-Zr-Y), the basalts are within-plate rocks.

The felsic volcanic rocks correspond to rhyolites with SiO_2 ~ 72 weight percent and (Na_2O+K_2O) ~ 9 weight percent (fig. 5). These rocks share many compositional characteristics with the granitic rocks of the Dashibalbar pluton. They are high in Fe and $Fe_{(tot)}/(Fe_{(tot)+}Mg)$ ratio but low in Mg and Al. Similarly, they are metaluminous with the A/NK values ~1.04 and A/CNK values ~0.9 although they can be classified according to Liegeois and others (1998) as alkaline. This is consistent with the study of Yarmolyuk and others (2002) who considered some of these rocks to be comendites. The felsic volcanic rocks have distinctly fractionated REE patterns with $(La/Yb)_n$ ~5 and $(Gd/Yb)_n$ ~ 1.2 and with pronounced negative Eu anomalies (fig. 9). Their

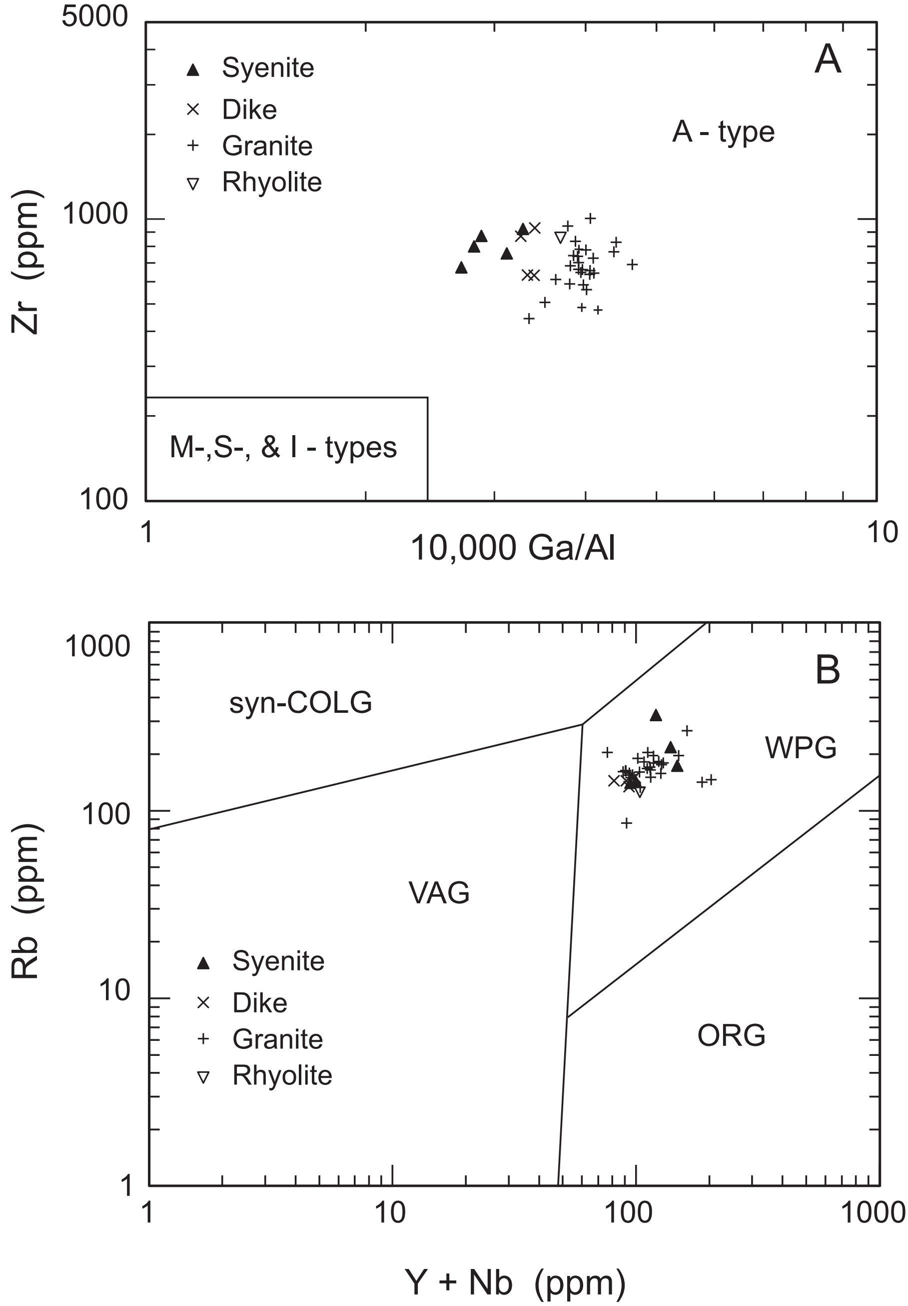

Fig. 8. (A) 10,000*Ga/Al versus Zr (ppm) discrimination diagram (after Whalen and others, 1987) for the Dashibalbar granitoids classifying the rocks as A-type granites. Fields: MSI field indicates the distribution of M-, S- and I-type granites while the A field is for the A-type granites. (B) Rb versus (Nb+Y) (ppm) diagram of Pearce and others (1984) for the granitic rocks of the Dashibalbar pluton. Fields: syn-COLG-syncollisional granite, VAG-volcanic arc granite, WPG-within-plate granite, ORG-ocean-ridge granite.

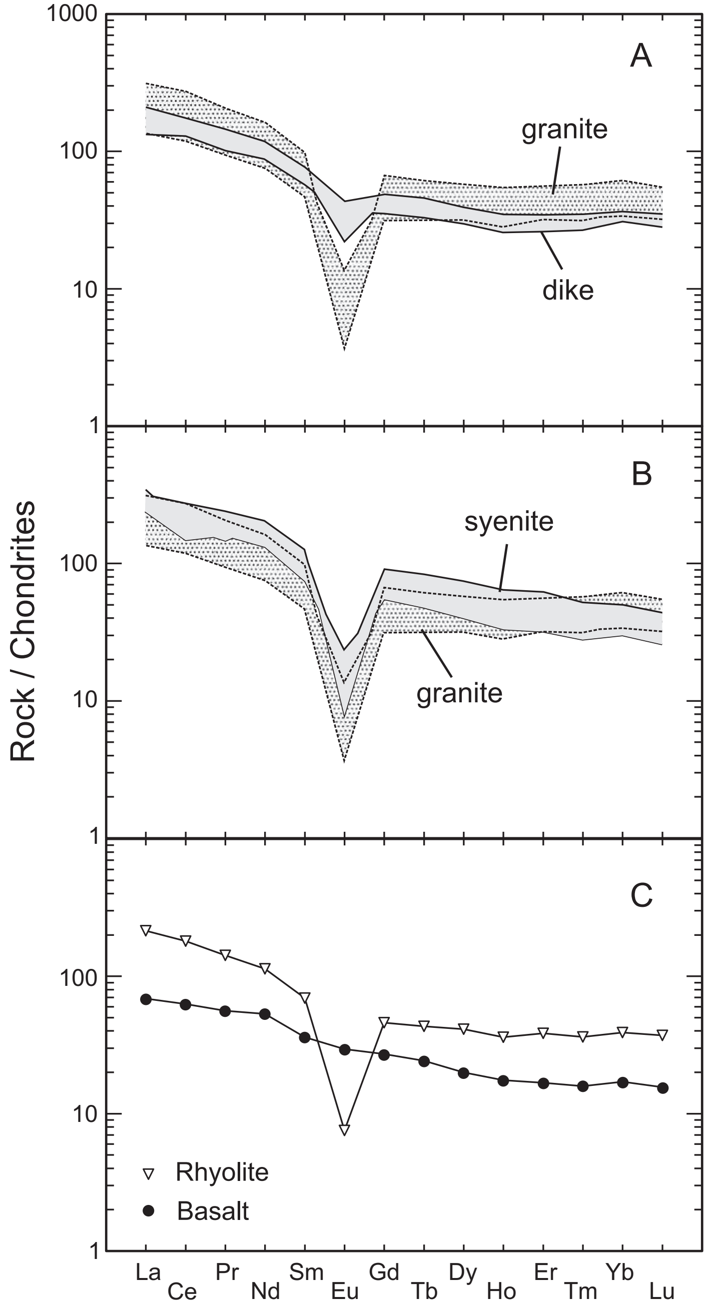

Fig. 9. Chondrite-normalized REE patterns of the Dashibalbar pluton and volcanic complex. (A) Ranges of granitic rocks and dikes of the pluton, (B) ranges of granitic rocks and syenitic enclaves of the pluton, (C) rhyolite (DB-22) and basalt (DB-21) of the volcanic complex. Normalizing values are after Sun and McDonough (1989).

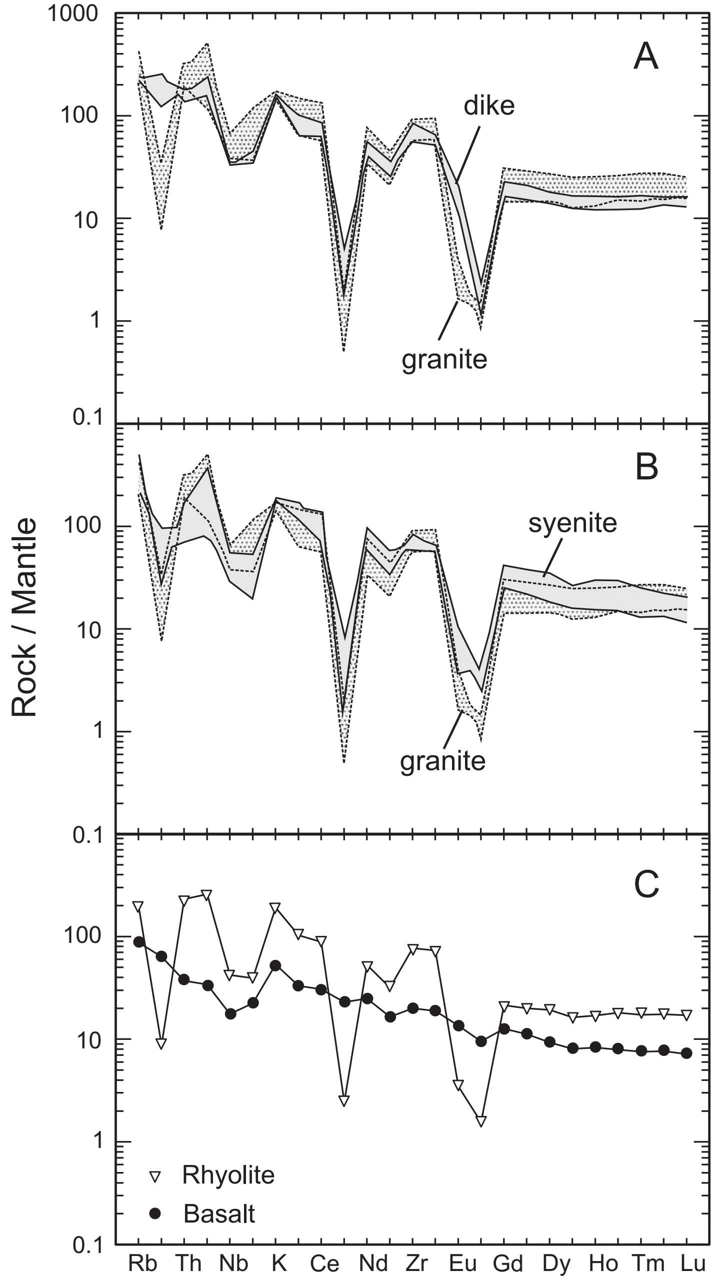

Fig. 10. Primitive mantle-normalized incompatible element patterns of the Dashibalbar pluton and volcanic complex. (A) Ranges of granitic rocks and dikes of the pluton, (B) ranges of granitic rocks and syenitic enclaves of the pluton, (C) rhyolite (DB-22) and basalt (DB-21) of the volcanic complex. Normalizing values are after Sun and McDonough (1989).

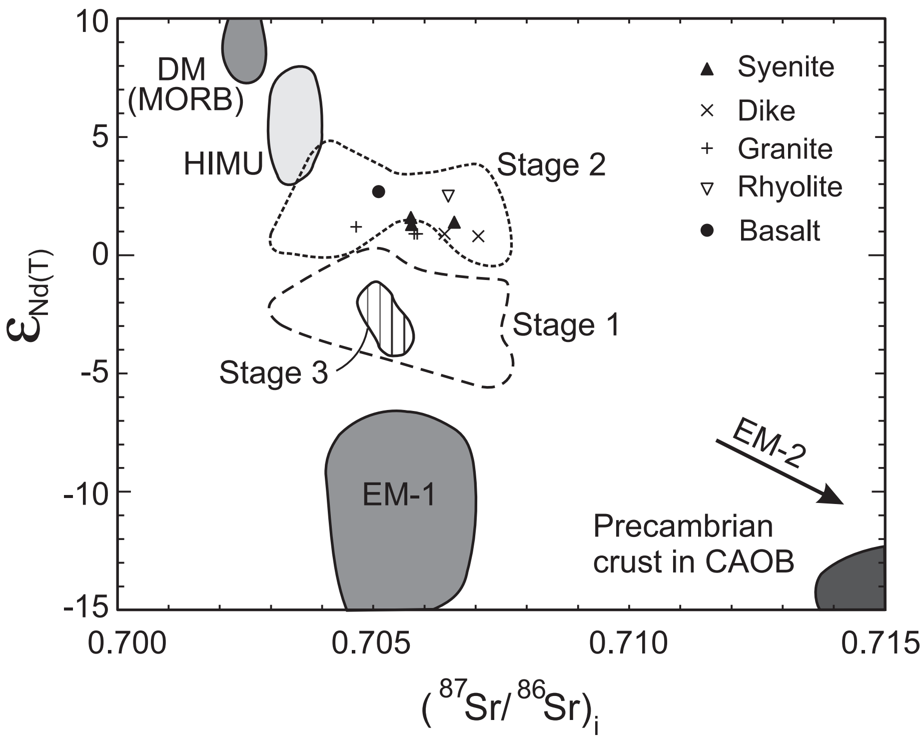

Fig. 11. $\varepsilon_{Nd(t)}$ versus $(^{87}Sr/^{86}Sr)_i$ diagram for the Dashibalbar pluton and volcanic complex. The fields of three stages of alkaline granitoid magmatism of the Mongolian-Transbaikalian belt as well as the Precambrian crust in the CAOB are from Jahn and others (2009). The principal mantle components of Zindler and Hart (1986) are shown for comparison. Three magmatic stages (Jahn and others, 2009) are 295 to 270 Ma (stage 1), 230 to 190 Ma (stage 2) and 150 to 120 Ma (stage 3).

primitive mantle-normalized pattern is characterized by distinct negative anomalies of Ti, Eu, Ba and Sr as well as small negative Nb and Ta anomalies (fig. 10). Both the chondrite- and primitive mantle-normalized patterns of the felsic volcanic rocks are sub-parallel to those of the granites. The felsic volcanic rocks have chemical characteristics of A-type, within-plate granites (fig. 8).

Isotopes

The Nd and Sr isotopic data are given in table 4. The initial isotopic ratios and $\varepsilon_{Nd(t)}$ values were all age-corrected to 186 Ma. The initial Sr isotopic values of the analyzed rocks vary in a range of 0.7047 to 0.7071 with the majority falling about 0.706. The values for all the rock groups are similar and overlap those compiled by Jahn and others (2009) for the Mesozoic alkaline granitoids and related volcanic complexes of the Mongolian-Transbaikalian igneous province (fig. 11). The initial Sr isotopic ratios are generally consistent with the Nd isotopic data (fig. 11). In some samples with high $^{87}Rb/^{86}Sr$ ratios, the calculated initial Sr isotopic ratios might have a significant error (for example Wu and others, 2002; Jahn and others, 2009).

The granites and dikes have a range of $\varepsilon_{Nd\ (186\ Ma)}$ values ($\sim$ +0.8 to +1.2) and T_{DM} model ages (~850-970 Ma). The enclaves have slightly higher $\varepsilon_{Nd(t)}$ values (+1.3 to +1.6) but overlapping the model ages (~800-900 Ma). The basalt and rhyolite of the bimodal sequence have similar positive $\varepsilon_{Nd(t)}$ values (+2.5 to +2.7), which are

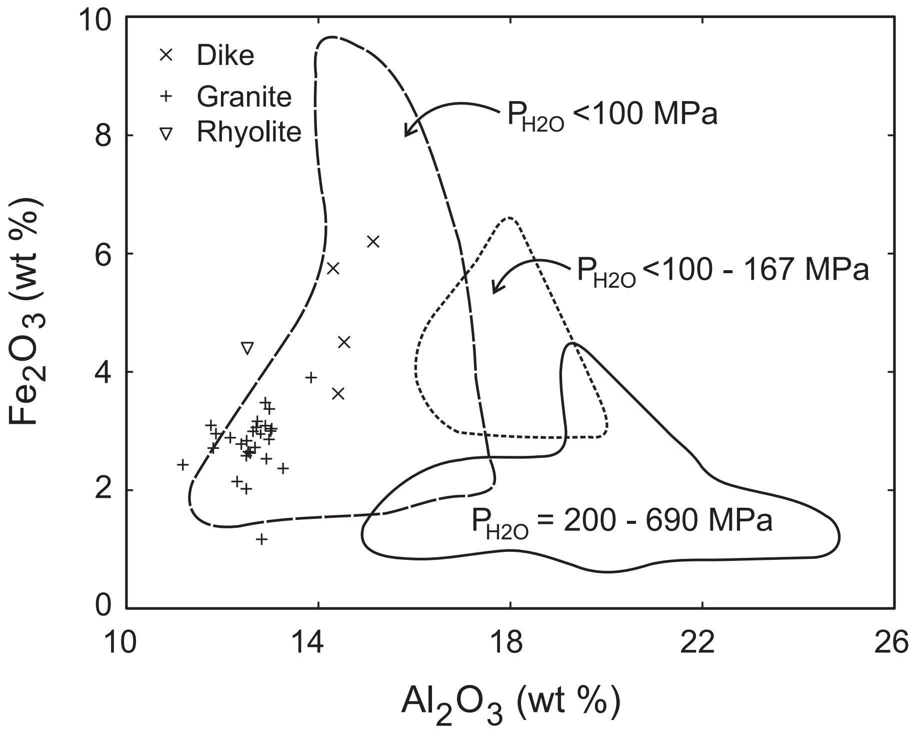

Fig. 12. Al_2O_3 versus $Fe_2O_{3\ (tot)}$ (wt.%) diagram for the felsic rocks of the Dashibalbar pluton showing the fields of experimentally generated granitic melt compositions at different P_{H2O} (after Beard, 1995 and Chaudhuri and others, 2003).

higher than those of the pluton. Their model ages (~800 Ma) are comparable to those of the intrusions and enclaves. All of these values, including $\varepsilon_{Nd(t)}$ and T_{DM}, are within the range of A-type granites of the Early Mesozoic Mongolian-Transbaikalian igneous province (fig. 11), in particular the intrusions of the stage 2 of Jahn and others (2009), the values of which range from −1 to +4. Jahn and others (2009) suggested that these rocks were derived either from a mantle source or from mantle-derived mafic rocks in the lower crust. The mantle source was mildly depleted as has been suggested for Early Mesozoic granitoids elsewhere in Mongolia (Jahn and others, 2009).

PETROGENESIS

A comparison of experimental data on the generation of granitic melts at various conditions of $P_{(H2O)}$ (fig. 12) with the relatively Al-poor and Fe-rich Dashibalbar granites suggests emplacement at relatively low initial water pressure conditions. However, the general occurrence of amphibole instead of pyroxene points to the existence of water in the magma, at least in late stages of its evolution. The partial replacement of early pyroxene by amphibole in some samples, and the restriction of relict plagioclase to (quartz) syenite enclaves, are attributed to increasing $P_{(H2O)}$ during fractionation due to both differentiation and assimilation. Thus, the Al and Fe abundances and the ferroan nature of the granites indicate that the rocks were generated at high temperature, but emplaced at shallow depth, and that the magma was initially relatively anhydrous and reduced in nature (compare Frost and others, 2001). Such conditions are generally considered to be common in the extensional tectonic regime that is responsible for the generation of many A-type granitoids (for example Frost and Frost, 2011).

The major and trace element variations of the granitic rocks of the Dashibalbar pluton are interpreted to reflect predominantly fractional crystallization. The strong depletion of Ba, Sr and Eu as shown in the spider diagrams and REE patterns are likely the result of fractional crystallization of feldspars during magma evolution.

The (quartz) syenitic rocks of the enclaves are spatially and probably temporally associated with the granites and show many common geochemical and mineralogical characteristics. Syenitic rocks are frequently present in the alkaline granitic complexes of the CAOB (for example Jahn and others, 2009), suggesting that both rock types are genetically related and that the granites could have been derived from a syenitic magma by magmatic differentiation. Fractionation of syenites, which compared to granites are higher in Al, Ca, Fe, Mg, Ti and alkalis but lower in silica, probably involved crystallization of alkali feldspar, plagioclase, amphibole and/or clinopyroxene. Most of the trends of the granitic and syenitic rocks are consistent with fractional crystallization, a process that may also be responsible for the variations within the individual rock suits of the intrusion. However, there are significant differences in incompatible trace element ratios including $(Gd/Yb)_n$, indicating that the granites were not derived from the syenite via continuous fractional crystallization. An alternative model to continuous fractional crystallization for the origin of the granites and their relation to the syenites is assimilation-fractional crystallization (AFC). The high Th/La ratios are sensitive indicators of crustal contamination (for example Sun and McDonough, 1989). Significant differences of these ratios in granites (typically ~0.2-0.4) with typical crustal values compared to those of syenites (typically ~0.1-0.11) with typical mantle values (~0.12; Sun and McDonough, 1989) suggest that the granites were contaminated by continental crust and the AFC process played a role during evolution of the granites from the syenitic magma. Subtle differences in the Nd isotopic values ($\varepsilon_{Nd[t]}$: +0.8 to +1.2 in granites versus +1.3 to +1.6 in syenites; table 4) and the presence of xenoliths of country rocks in the granites are consistent with such a process. However, the crustal contaminant was likely silicic.

Assuming that the granites were derived from a syenitic parent magma, the question arises as to the origin of the syenite. The genesis of syenites is still controversial. Commonly proposed models for the origin of syenites are (1) partial melting of metasomatized mantle (for example Lynch and others, 1993; Platt, 1996), (2) differentiation of alkali/transitional basaltic magmas (Thorpe and Tindle, 1992; Civetta and others, 1998; Ronga and others, 2010), (3) melting of underplated basalts (Sisson and others, 2005; Bonin, 2007; Jahn and others, 2009) and (4) magma mixing, typically mantle-derived basic magma with silicic crustal melts (for example Marks and Markl, 2001).

Litvinovsky and others (1999) and Jahn and others (2009) argued that mixing of mantle-derived mafic magma with silicic crustal melts, followed by subsequent differentiation (for example Zhao and others, 1995) is not a viable mechanism as it requires an unusual proportion of end-members. According to the geochemical and isotopic characteristics of the syenitic rocks, the parent alkaline silicic magma was derived either from an enriched mantle source or from enriched mantle-derived mafic rocks in the lower crust. A comparison with similar rocks elsewhere, including recent trachytic rocks (for example Civetta and others, 1998; Ronga and others, 2010), suggests that the syenitic rocks were generated either by partial melting or fractional crystallization of mildly alkali or transitional basalts (Brown and Becker, 1986; Thorpe and Tingle, 1992). Such an origin is also consistent with the distribution of granitic and syenitic rocks on the trace element discrimination diagrams of Eby (1992) where the Dashibalbar granitoid rocks plot into the A2 fields (fig. 13). Derivation of syenites from an

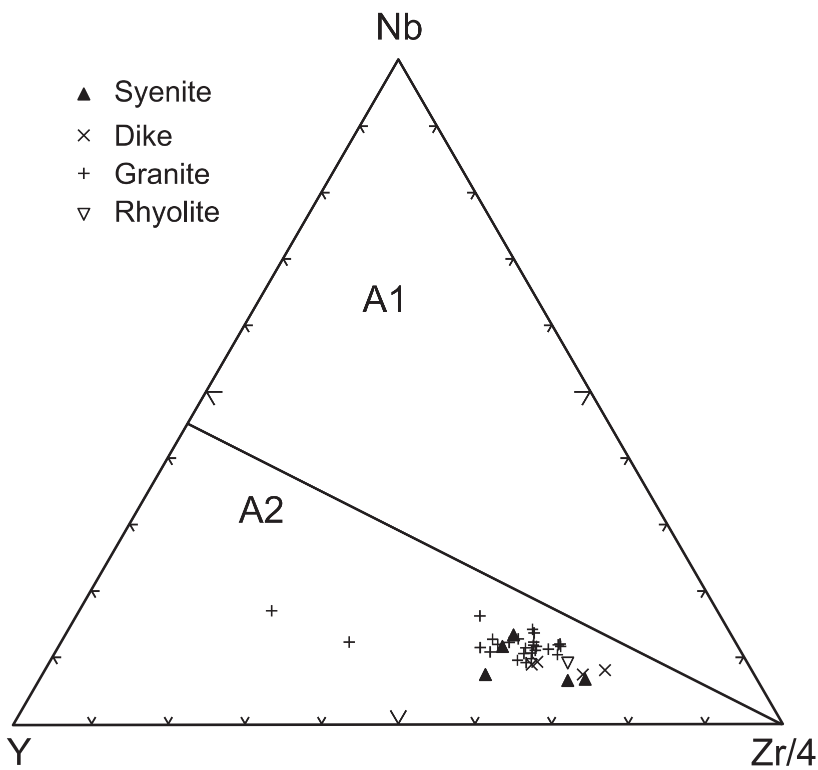

Fig. 13. Y-Nb-Zr/4 diagrams of Eby (1992) for the felsic rocks of the Dashibalbar igneous complex, showing the fields of the A1- and A2-type granitoids.

enriched mantle-derived basaltic source can probably be invoked for many other alkaline silicic rocks of the Mongolian-Transbaikalian igneous province of CAOB (Jahn and others, 2009).

Geochemical characteristics of basalts of the Dashibalbar bimodal volcanic complex, including distinct enrichment of incompatible elements, presence of a negative Nb anomaly on mantle-normalized plots and Nd-isotopic values are indicative of a subcontinental lithospheric mantle source. The felsic volcanic rocks are compositionally similar to the granites but are not closely related to them. Although they were derived from a similar source/magma, their evolution paths were different.

TECTONIC IMPLICATIONS AND CONCLUSIONS

The *ca.* 186 Ma Dashibalbar pluton occurs in the North-Gobi rift and is *ca.* 9 my younger than the 225 to 195 Ma Khentey batholith, which suggests that igneous activity lasted in the area a little longer than proposed by Yarmolyuk and Kuzmin (2011). Our data suggest that the Dashibalbar magma was derived from an underlying Neoproterozoic mafic crust (underplated transitional or mildly alkaline basalts) and subcontinental lithospheric mantle (Dashibalbar basalt). Megablocks of the Neoproterozoic crust are exposed in adjacent parts of the CAOB (Bogdanov and others, 1998; Vernikovsky and others, 2009; Reichow and others, 2010; Wilhem and others, 2012). Compositional and isotopic similarities of A-type granites and syenites over a large area of CAOB support such an origin.

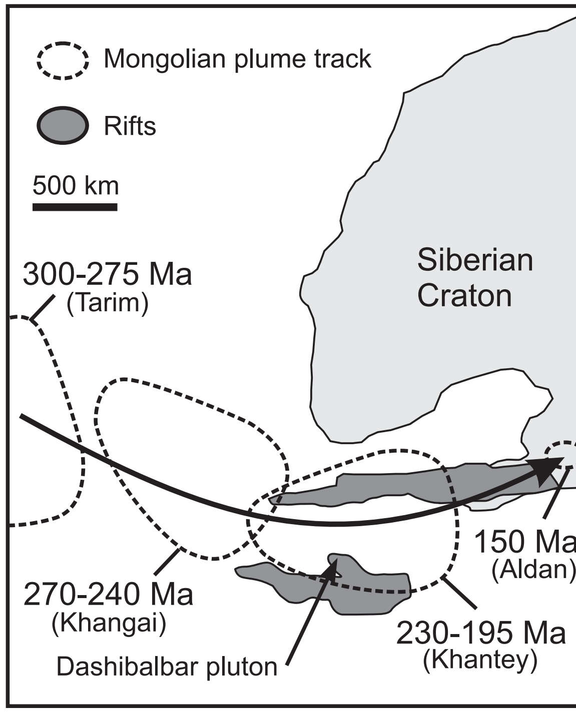

Fig. 14. Reconstruction of the movement of the Mongolian mantle plume and magmatic activities related to the rift systems in Eastern Mongolia and Transbaikalia resulting from the rotation of the Siberian continent over the Mongolian plume (after Yarmolyuk and Kuzmin, 2011). Dashed lines delineate the positions of the Mongolian plume at 300 to 275 Ma, 270 to 240 Ma, 230 to 195 Ma and 150 Ma; the arrow is a tracer of Mongolian plume while the dark fields outline the North-Gobi and Western-Trans-Baikalian rifts.

The generation of alkaline felsic/intermediate magmas needs a temperature of ≥950 °C for dehydration melting of amphibolite (Rapp and Watson, 1995), which requires the rise of a heat source. Such a heat source can be provided by thinning of the lithosphere during rifting, delamination of the lower lithosphere, and a mantle plume. Distinguishing between these tectonic models is difficult, especially from a single pluton; regional temporal/spatial relationships are essential criteria. The association of normal (subalkaline)–alkaline magmatism with NE-trending rift zones is consistent with a rifting mechanism. However, the large scale melting and the eastward migration of the magmatic centre through time (fig. 14) from Tarim-South Mongolia at 300 to 275 Ma when the Tarin trap basalts were extruded (Yu and others, 2011), through the Khangai area at 270 to 240 Ma to the Khentey area of Eastern Mongolia and Transbaikalia at 230 to 195 Ma to Aldan-Zeisky at 150 Ma are consistent with the migration over a stationary mantle plume (the Mongolian plume of Kuzmin and others, 2010; Yarmolyuk and Kuzmin, 2011 and Derbeko, 2012). Migration of Mongolia over a mantle plume is consistent with paleomagnetic data (Kuzmin and others, 2010). The Mongolian plume would provide the heat source for the magmatism (fig. 14), and would account for its zonal nature which grades from normal granitoids in the center of the Khentey batholith through Li-F granites towards the batholith margins to alkaline and peralkaline intrusions and lavas in the marginal rifts (Yarmolyuk and Kuzmin, 2011). Thus, the crust above the plume is more extensively melted in comparison to the margins where deeper and less extensive melting took place. To date, no asthenospheric magma from the plume has been identified; however, the rare gabbros require more detailed study to determine their origin.

ACKNOWLEDGMENTS

We thank the guest editors of this special issue for their invitation to contribute this paper. We acknowledge a support from UPCD-CIDA Tier 2 project as well as a Natural Sciences and Engineering Research Council (Canada) Discovery grant to JD. We are also grateful to Dr. Ulf Linnemann for facilitating zircon dating and Dr. S. Amar-Amgalan from Department of Geology, Mongolian University of Science and Technology, for providing assistance during field work. Alfred Kröner, Sun-Lin Chung, and Boris Litvinovsky are thanked for reviews of the manuscript that resulted in an improved final version.

APPENDIX 1

GEOCHRONOLOGY

TABLE A1

LA-ICP-MS U-Pb isotopic data of zircons from amphibole granite

Number	$^{207}Pb^{a}$ (cps)	U^{b} (ppm)	Pb^{b} (ppm)	Th^{b}/U	$^{206}Pb^{c}/^{204}Pb$	$^{206}Pb^{c}/^{238}U$	2 σ %	$^{207}Pb^{c}/^{235}U$	2 σ %	$^{207}Pb^{c}/^{206}Pb$	2 σ %	rho[d]	$^{206}Pb/^{238}U$	2 σ (Ma)	$^{207}Pb/^{235}U$	2 σ (Ma)	$^{207}Pb/^{206}Pb$	2 σ (Ma)	conc %
a1	2205	114	4	0.42	870	0.03334	1.7	0.37070	9.4	0.08063	9.3	0.18	211	4	320	26	1212	182	17
a2	4163	158	6	0.42	266	0.02893	2.0	0.42616	8.1	0.10683	7.8	0.25	184	4	360	25	1746	143	11
a3	1400	98	3	0.42	1840	0.02800	2.0	0.24412	6.1	0.06323	5.7	0.33	178	3	222	12	716	122	25
a4	2444	194	6	0.33	3451	0.02953	2.6	0.21283	4.6	0.05228	3.9	0.55	188	5	196	8	297	88	63
a5	1367	122	4	0.30	2749	0.02881	1.6	0.19711	6.1	0.04963	5.9	0.26	183	3	183	10	178	139	**103**
a6	1709	130	4	0.36	2916	0.02925	2.0	0.23551	4.5	0.05839	4.0	0.45	186	4	215	9	544	88	34
a7	1972	153	5	0.40	3574	0.03251	1.7	0.24871	4.2	0.05548	3.8	0.40	206	3	226	9	431	86	48
a8	2517	137	5	0.60	554	0.03010	1.8	0.35583	6.2	0.08573	5.9	0.29	191	3	309	17	1332	114	14
a9	1503	111	4	0.35	2534	0.02998	1.8	0.24556	4.5	0.05941	4.2	0.40	190	3	223	9	582	90	33
a10	30983	1906	55	0.14	665	0.02737	2.2	0.18904	3.7	0.05009	2.9	0.61	174	4	176	6	199	68	87
a11	6018	81	5	0.37	70	0.03633	1.8	1.31429	5.6	0.26240	5.3	0.32	230	4	852	33	3261	84	7
a12	4094	192	6	0.41	331	0.02835	2.3	0.38872	6.5	0.09943	6.1	0.35	180	4	333	19	1613	114	11
a13	1239	113	3	0.39	1264	0.02878	2.5	0.19733	5.7	0.04973	5.1	0.44	183	4	183	10	183	119	**100**
a14	2156	201	7	0.57	4354	0.03036	1.6	0.20696	4.0	0.04945	3.7	0.39	193	3	191	7	169	86	114
a15	1207	110	3	0.39	2290	0.03023	2.4	0.22009	5.6	0.05280	5.0	0.44	192	5	202	10	320	115	60
a16	1609	133	5	0.63	1582	0.03225	1.8	0.24088	6.3	0.05418	6.1	0.29	205	4	219	13	378	136	54
a17	1344	131	4	0.40	2693	0.02906	1.7	0.19936	6.1	0.04976	5.8	0.28	185	3	185	10	184	135	**101**
a18	1957	136	4	0.60	766	0.02701	2.3	0.25782	5.7	0.06924	5.2	0.40	172	4	233	12	906	108	19
a19	4602	100	5	0.44	126	0.03615	3.9	0.84374	10.7	0.16928	10.0	0.36	229	9	621	51	2551	168	9
a20	1297	124	4	0.39	1522	0.02963	1.7	0.20440	4.5	0.05003	4.2	0.37	188	3	189	8	196	97	**96**
a21	1304	124	4	0.34	2482	0.02956	1.8	0.21376	5.3	0.05245	5.0	0.35	188	3	197	10	305	114	62
a22	1948	122	4	0.39	370	0.03057	2.6	0.32261	9.8	0.07654	9.5	0.26	194	5	284	25	1109	189	17
a23	1019	90	3	0.39	1631	0.03170	2.6	0.24638	7.7	0.05637	7.2	0.34	201	5	224	15	467	160	43
a24	2215	172	5	0.34	3136	0.02908	1.8	0.28243	3.8	0.07044	3.4	0.47	185	3	253	9	941	69	20
a25	1582	77	2	0.34	206	0.02635	1.9	0.35882	9.5	0.09878	9.3	0.20	168	3	311	26	1601	173	10
a26	2550	137	5	0.38	257	0.03055	1.6	0.37286	12.8	0.08852	12.7	0.12	194	3	322	36	1394	244	14
a27	1422	148	5	0.46	2840	0.02949	1.4	0.20289	4.4	0.04990	4.2	0.31	187	3	188	8	190	97	98

TABLE A1
(continued)

Number	$^{207}Pb^{a}$ (cps)	U^{b} (ppm)	Pb^{b} (ppm)	Th^{b}/U	$^{206}Pb^{c}/^{204}Pb$	$^{206}Pb^{c}/^{238}U$	2 σ %	$^{207}Pb^{c}/^{235}U$	2 σ %	$^{207}Pb^{c}/^{206}Pb$	2 σ %	rho[d]	$^{206}Pb/^{238}U$	2 σ (Ma)	$^{207}Pb/^{235}U$	2 σ (Ma)	$^{207}Pb/^{206}Pb$	2 σ (Ma)	conc %
a29	2422	100	3	0.35	339	0.02511	2.7	0.22401	20.1	0.06470	19.9	0.13	160	4	205	38	765	420	21
a30	1528	111	3	0.40	1890	0.02705	1.7	0.25407	7.9	0.06812	7.7	0.22	172	3	230	16	872	160	20
a31	5613	75	8	0.71	71	0.06875	2.9	2.34797	23.1	0.24768	22.9	0.12	429	12	1227	180	3170	364	14
a32	799	79	2	0.43	777	0.02915	3.5	0.22296	7.7	0.05548	6.9	0.45	185	6	204	14	432	153	43
a33	1018	114	3	0.38	595	0.02922	2.8	0.20149	6.2	0.05002	5.6	0.44	186	5	186	11	196	130	**95**
a34	899	95	3	0.43	1715	0.02821	2.8	0.20385	6.6	0.05241	6.0	0.43	179	5	188	11	303	137	59
a35	1014	100	3	0.45	1770	0.02695	1.8	0.21308	8.0	0.05734	7.8	0.22	171	3	196	14	505	173	34
a36	1719	146	5	0.66	1069	0.02964	1.6	0.26962	6.3	0.06597	6.1	0.26	188	3	242	14	805	127	23
a37	1409	131	4	0.46	2407	0.02768	2.6	0.22342	8.1	0.05854	7.6	0.33	176	5	205	15	550	166	32
a38	1771	140	5	0.82	1357	0.02928	1.7	0.24698	7.1	0.06118	6.9	0.24	186	3	224	14	646	147	29
a39	1090	106	3	0.29	938	0.02876	1.4	0.19716	6.4	0.04973	6.2	0.22	183	2	183	11	182	145	**100**
a40	510	42	1	0.34	960	0.02898	2.7	0.21748	10.0	0.05443	9.6	0.27	184	5	200	18	389	216	47
a41	807	69	2	0.32	1610	0.02949	2.4	0.20347	6.7	0.05005	6.3	0.36	187	4	188	12	197	146	**95**
a42	1014	84	3	0.36	2032	0.02958	2.3	0.20348	4.6	0.04988	4.0	0.50	188	4	188	8	190	93	**99**
a43	1133	89	3	0.38	2220	0.02875	2.2	0.20369	5.9	0.05139	5.5	0.38	183	4	188	10	258	125	71
a44	1574	105	3	0.31	1377	0.02962	1.6	0.23298	7.7	0.05704	7.5	0.21	188	3	213	15	493	166	38
a45	1548	92	3	0.33	1592	0.02961	2.2	0.25269	7.7	0.06190	7.4	0.28	188	4	229	16	671	159	28
a46	1532	102	3	0.41	667	0.02736	2.1	0.20559	4.1	0.05450	3.5	0.51	174	4	190	7	392	79	44
a47	1288	92	3	0.32	2583	0.02878	2.3	0.19746	5.8	0.04976	5.3	0.40	183	4	183	10	184	123	99
a48	1398	60	2	0.39	427	0.02682	3.2	0.26022	8.0	0.07036	7.3	0.40	171	5	235	17	939	150	18
a49	513	32	1	0.31	1027	0.02954	2.5	0.20322	6.6	0.04989	6.1	0.38	188	5	188	11	190	141	99
a50	814	48	1	0.35	1639	0.02884	2.2	0.19793	5.3	0.04977	4.9	0.41	183	4	183	9	184	113	99
a51	11408	538	16	0.27	1917	0.02891	1.7	0.19836	4.5	0.04977	4.1	0.38	184	3	184	8	184	96	100
a52	1501	76	3	0.38	458	0.03237	3.8	0.27110	9.1	0.06075	8.3	0.41	205	8	244	20	630	179	33
a53	549	28	1	0.38	1059	0.03174	1.9	0.22729	8.5	0.05194	8.2	0.22	201	4	208	16	283	189	71
a54	3387	61	3	0.31	241	0.03217	3.2	0.56992	13.2	0.12850	12.8	0.25	204	7	458	50	2078	225	10

Table A1
(continued)

Number	$^{207}Pb^{a}$ (cps)	U^{b} (ppm)	Pb^{b} (ppm)	Th^{b}/U	$^{206}Pb^{c}/^{204}Pb$	$^{206}Pb^{c}/^{238}U$	2 σ %	$^{207}Pb^{c}/^{235}U$	2 σ %	$^{207}Pb^{c}/^{206}Pb$	2 σ %	rho[d]	$^{206}Pb/^{238}U$	2 σ (Ma)	$^{207}Pb/^{235}U$	2 σ (Ma)	$^{207}Pb/^{206}Pb$	2 σ (Ma)	conc %
a55	477	23	1	0.34	955	0.02979	3.2	0.20493	8.6	0.04990	8.0	0.37	189	6	189	15	190	185	**99**
a56	1072	39	1	0.47	421	0.03200	2.0	0.31447	10.0	0.07128	9.8	0.20	203	4	278	25	965	200	21
a57	1060	33	1	0.42	1276	0.02830	1.7	0.32375	5.8	0.08296	5.5	0.29	180	3	285	14	1268	108	14
a58	623	30	1	0.30	1245	0.02976	1.6	0.20472	7.5	0.04988	7.4	0.21	189	3	189	13	190	172	**100**
a59	1259	50	2	0.38	1988	0.03528	2.7	0.30439	9.4	0.06257	9.0	0.29	224	6	270	23	694	192	32
a60	346	15	1	0.39	674	0.03239	1.5	0.23575	8.5	0.05279	8.4	0.17	205	3	215	17	320	190	64
b1	867	88	3	0.62	1676	0.02711	3.8	0.19395	9.4	0.05188	8.6	0.40	172	6	180	16	280	197	62
b2	1594	59	2	0.50	295	0.03078	3.8	0.50434	17.0	0.11884	16.6	0.22	195	7	415	60	1939	297	10
b3	987	86	3	0.60	1677	0.02717	2.7	0.22073	6.9	0.05893	6.3	0.39	173	5	203	13	565	137	31
b4	844	64	2	0.88	1259	0.02500	3.5	0.23305	7.9	0.06760	7.1	0.44	159	6	213	15	856	147	19
b5	601	52	2	0.34	1027	0.02919	2.5	0.23645	7.4	0.05875	7.0	0.33	185	5	216	15	558	153	33
b6	185	7	0	0.44	4	0.04357	9.3	0.70275	76.0	0.11698	75.4	0.12	275	25	540	382	1911	1354	14
b7	1156	33	1	0.65	285	0.02610	7.0	0.76216	15.5	0.21183	13.9	0.45	166	12	575	71	2920	224	6
b8	884	63	3	0.92	989	0.03803	3.0	0.48326	21.1	0.09216	20.9	0.14	241	7	400	72	1471	397	16
b9	586	29	1	0.44	558	0.03763	2.6	0.52932	21.9	0.10202	21.7	0.12	238	6	431	80	1661	402	14
b10	1359	44	2	0.95	394	0.02878	4.8	0.80819	26.0	0.20369	25.6	0.18	183	9	601	126	2856	416	6
b11	1197	69	2	0.30	321	0.03147	2.5	0.37273	7.6	0.08589	7.1	0.33	200	5	322	21	1336	138	15
b12	1177	95	3	0.56	1437	0.02847	2.3	0.25894	5.2	0.06597	4.7	0.43	181	4	234	11	806	99	22
b13	1027	70	3	0.38	451	0.03468	2.2	0.34506	13.0	0.07217	12.8	0.17	220	5	301	34	991	260	22
b14	4061	316	10	0.37	520	0.02922	2.0	0.27835	5.6	0.06908	5.2	0.36	186	4	249	13	901	108	21
b15	563	46	2	0.48	819	0.03120	3.3	0.29602	10.8	0.06881	10.3	0.30	198	6	263	25	893	213	22
b16	638	36	1	0.65	603	0.02932	3.1	0.42929	12.1	0.10620	11.6	0.26	186	6	363	37	1735	214	11
b17	1093	120	4	0.34	2176	0.02958	1.6	0.20553	4.5	0.05039	4.2	0.36	188	3	190	8	213	98	88
b18	1062	127	4	0.41	2124	0.02972	2.1	0.20507	5.9	0.05005	5.5	0.36	189	4	189	10	197	128	**96**
b19	1194	105	3	0.41	1766	0.03051	1.9	0.24993	5.2	0.05942	4.9	0.36	194	4	227	11	582	106	33
b20	957	108	4	0.52	1919	0.02956	2.7	0.20341	5.4	0.04991	4.6	0.51	188	5	188	9	191	107	98
b21	1127	142	4	0.36	2267	0.02864	2.3	0.19667	4.9	0.04981	4.3	0.46	182	4	182	8	186	100	98

TABLE A1
(continued)

Number	$^{207}Pb^{a}$ (cps)	U^{b} (ppm)	Pb^{b} (ppm)	Th^{b}/U	$^{206}Pb^{c}/^{204}Pb$	$^{206}Pb^{c}/^{238}U$	2 σ %	$^{207}Pb^{c}/^{235}U$	2 σ %	$^{207}Pb^{c}/^{206}Pb$	2 σ %	rho^{d}	$^{206}Pb/^{238}U$	2 σ (Ma)	$^{207}Pb/^{235}U$	2 σ (Ma)	$^{207}Pb/^{206}Pb$	2 σ (Ma)	conc %
b22	1436	141	4	0.53	542	0.02610	2.1	0.21799	5.6	0.06057	5.2	0.37	166	3	200	10	624	113	27
b23	1500	114	4	0.38	340	0.02744	3.0	0.29150	8.3	0.07705	7.7	0.36	175	5	260	19	1122	154	16
b24	1329	140	4	0.37	1387	0.02845	1.8	0.21694	6.0	0.05530	5.7	0.30	181	3	199	11	424	127	43
b25	183386	2088	194	0.20	54	0.06506	2.6	0.49183	11.5	0.05483	11.3	0.22	406	10	406	39	405	252	**100**
b26	1381	88	4	0.66	308	0.03274	3.7	0.43746	20.1	0.09692	19.8	0.18	208	7	368	64	1566	371	13
b27	1824	137	5	0.44	217	0.03086	4.5	0.30427	7.9	0.07150	6.5	0.57	196	9	270	19	972	132	20
b28	1362	167	5	0.37	2731	0.02959	1.7	0.20387	5.0	0.04997	4.7	0.34	188	3	188	9	194	109	**97**
b29	1067	112	4	0.55	601	0.02898	2.5	0.23070	7.0	0.05773	6.6	0.35	184	4	211	13	520	145	35
b30	1787	179	6	0.26	819	0.03072	2.1	0.25902	5.6	0.06116	5.2	0.38	195	4	234	12	645	112	30
b31	1353	136	4	0.41	2237	0.02876	1.7	0.24109	5.4	0.06081	5.1	0.32	183	3	219	11	632	111	29
b32	1128	89	3	0.46	1164	0.02804	2.6	0.29573	9.4	0.07650	9.0	0.28	178	5	263	22	1108	179	16
b33	1806	172	5	0.43	932	0.02455	1.9	0.23196	5.0	0.06853	4.7	0.38	156	3	212	10	885	96	18
b34	3015	315	10	0.29	1018	0.03072	2.0	0.22846	3.9	0.05393	3.3	0.52	195	4	209	7	368	75	53
b35	1503	201	6	0.49	2994	0.02908	1.9	0.20180	4.8	0.05034	4.5	0.39	185	3	187	8	211	103	88
b36	1336	147	5	0.45	2230	0.03072	2.2	0.25307	6.1	0.05975	5.7	0.36	195	4	229	13	594	123	33
b37	1198	104	4	0.59	556	0.02786	2.4	0.26565	11.2	0.06916	11.0	0.21	177	4	239	24	903	226	20
b38	1810	155	5	0.62	927	0.02798	1.9	0.29100	5.8	0.07544	5.5	0.32	178	3	259	13	1080	110	16
b39	1544	129	4	0.35	758	0.02884	2.6	0.26614	6.0	0.06694	5.4	0.43	183	5	240	13	836	112	22
b40	2190	239	8	0.64	4389	0.02889	1.8	0.19868	3.7	0.04989	3.3	0.48	184	3	184	6	190	76	**97**
b41	2042	137	5	0.50	632	0.03057	2.4	0.30873	4.6	0.07324	4.0	0.51	194	5	273	11	1021	81	19
b42	2220	152	5	0.65	800	0.03095	2.0	0.30015	5.4	0.07033	5.0	0.37	197	4	267	13	938	102	21
b43	1292	101	3	0.41	926	0.02775	1.9	0.22378	6.5	0.05848	6.2	0.29	176	3	205	12	548	135	32
b44	1080	93	3	0.52	2172	0.02983	2.8	0.20527	7.3	0.04991	6.8	0.39	189	5	190	13	191	157	**99**
b45	1247	87	3	0.34	2122	0.02901	2.6	0.23569	6.1	0.05893	5.5	0.43	184	5	215	12	565	120	33
b46	1988	75	3	0.41	234	0.03224	1.5	0.46926	12.2	0.10558	12.1	0.12	205	3	391	40	1724	222	12
b47	885	67	2	0.96	1783	0.02618	2.2	0.18013	7.5	0.04990	7.2	0.30	167	4	168	12	191	167	87

Table A1
(continued)

Number	$^{207}Pb^{a}$ (cps)	U^{b} (ppm)	Pb^{b} (ppm)	Th^{b}/U	$^{206}Pb^{c}/^{204}Pb$	$^{206}Pb^{c}/^{238}U$	2 σ %	$^{207}Pb^{c}/^{235}U$	2 σ %	$^{207}Pb^{c}/^{206}Pb$	2 σ %	rho[d]	$^{206}Pb/^{238}U$	2 σ (Ma)	$^{207}Pb/^{235}U$	2 σ (Ma)	$^{207}Pb/^{206}Pb$	2 σ (Ma)	conc %
b22	1436	141	4	0.53	542	0.02610	2.1	0.21799	5.6	0.06057	5.2	0.37	166	3	200	10	624	113	27
b48	1891	60	2	0.56	165	0.02846	3.6	0.42636	7.8	0.10867	6.9	0.46	181	6	361	24	1777	126	10
b49	688	60	2	0.44	1777	0.02882	2.0	0.15422	10.7	0.03881	10.5	0.18	183	4	146	15	-430	277	-43
b50	2688	73	3	0.36	236	0.02969	2.4	0.50723	7.7	0.12392	7.3	0.31	189	4	417	27	2013	130	9
b51	1028	64	2	0.47	1818	0.02780	2.6	0.21794	6.8	0.05685	6.3	0.39	177	5	200	12	486	139	36
b52	1336	73	2	0.40	2155	0.02850	1.9	0.24395	5.6	0.06209	5.3	0.34	181	3	222	11	677	112	27
b53	621	37	1	0.52	1248	0.02907	2.0	0.20031	6.7	0.04997	6.4	0.29	185	4	185	11	194	150	**95**
b54	1932	99	3	0.39	2071	0.02853	2.1	0.23277	4.9	0.05917	4.4	0.43	181	4	212	9	573	97	32
b55	4136	95	4	0.62	201	0.03562	2.7	0.61390	9.1	0.12499	8.7	0.29	226	6	486	36	2029	154	11
b56	1573	60	2	0.60	457	0.03169	2.6	0.33578	5.6	0.07686	4.9	0.46	201	5	294	14	1117	99	18
b57	5422	154	5	0.46	683	0.02968	1.7	0.20445	10.8	0.04997	10.6	0.16	189	3	189	19	193	247	**97**
b58	1620	93	3	0.37	3248	0.02644	2.8	0.18301	11.4	0.05020	11.1	0.25	168	5	171	18	204	257	82
b59	859	40	1	0.41	1499	0.02975	2.5	0.23558	6.6	0.05744	6.2	0.37	189	5	215	13	509	136	37
b60	1572	55	2	0.49	414	0.02483	1.9	0.24816	7.6	0.07248	7.4	0.25	158	3	225	16	999	150	16

[a] Within-run background-corrected mean ^{207}Pb signal in counts per second.
[b] U and Pb content and Th/U ratio were calculated relative to GJ-1 and are accurate to approximately 10%.
[c] Corrected for background, mass bias, laser induced U-Pb fractionation and common Pb (if detectable, see analytical method) using Stacey and Kramers (1975) model Pb composition. $^{207}Pb/^{235}U$ calculated using $^{207}Pb/^{206}Pb/(^{238}U/^{206}Pb \times 1/137.88)$. Errors are propagated by quadratic addition of within-run errors (2SE) and the reproducibility of GJ-1 (2SD).
[d] Rho is the error correlation defined as $err^{206}Pb/^{238}U/err^{207}Pb/^{235}U$.

Appendix 2
Major and trace element compositions of the rocks not included in table 2

Table A2

Major and trace element composition of the rocks of the Dashibalbar igneous complex

	Granite							
Sample	DB-3	DB-4	DB-5	DB-8	DB-9	DB-10	DB-12	DB-14
SiO_2 (%)	75.84	76.68	74.71	75.18	75.57	75.56	72.52	74.46
TiO_2	0.23	0.34	0.28	0.27	0.23	0.31	0.31	0.26
Al_2O_3	11.00	11.70	12.74	12.29	12.35	12.52	13.66	12.43
$Fe_2O_3{}^*$	2.39	3.08	3.17	2.79	2.55	2.65	3.85	2.63
MnO	0.01	0.02	0.07	0.04	0.04	0.04	0.07	0.04
MgO	0.05	0.07	0.05	0.09	0.11	0.12	0.07	0.11
CaO	1.53	0.06	0.08	0.03	0.14	0.12	0.24	0.36
Na_2O	3.13	3.51	4.22	2.51	3.58	4.24	2.89	3.92
K_2O	4.14	3.99	4.73	5.02	4.17	4.27	4.96	4.85
P_2O_5	0.09	0.04	0.05	0.05	0.04	0.07	0.06	0.04
LOI	1.19	0.52	0.55	0.79	0.55	0.35	0.70	0.49
SUM	99.60	100.01	100.64	99.06	99.33	100.25	99.33	99.60
Ni (ppm)	6	6	7	5	4	5	3	5
V	12	9	12	15	10	14	10	12
Zn	113	135	128	151	128	106	109	111
Rb	144	141	171	262	178	150	153	188
Ba	135	131	152	166	178	225	1423	229
Sr	22	14	13	14	22	28	64	37
Ga	23	23	27	26	25	23	26	26
Ta				4.7	2.9		1.8	2.2
Nb	40.0	54.4	34.1	47.0	36.0	39.6	22.9	32.6
Hf				28.6	19.0		16.0	18.6
Zr	478	941	637	990	675	506	603	641
Y	160	132	80	112	92	75	70	68
Th	55.8	45.0	24.1	26.4	19.0	22.3	15.3	20.7
U	5.9	8.8	3.8	7.6	4.3	6.2	4.1	2.8
La	120.4	113.0	69.2	100.0	71.9	89.8	70.8	76.0
Ce	227.2	201.3	206.4	232.0	156.5	174.3	132.4	171.5
Pr				26.18	19.88		18.76	19.91
Nd				101.0	80.0		75.1	77.1
Sm				19.47	15.58		14.40	14.75
Eu				0.43	0.35		2.24	0.41
Gd				17.93	14.93		12.95	12.51
Tb				3.01	2.79		2.11	2.13
Dy				19.33	17.44		12.56	13.05
Ho				4.08	3.52		2.43	2.66
Er				12.25	10.14		7.28	7.67
Tm				1.98	1.55		1.08	1.23
Yb				13.14	10.38		7.42	8.01
Lu				1.81	1.39		1.05	1.15
A/NK	1.14	1.16	1.06	1.29	1.19	1.08	1.35	1.06
A/CNK	0.89	1.15	1.04	1.28	1.16	1.06	1.29	1.01
Eu/Eu*				0.07	0.07		0.50	0.09
$(La/Yb)_n$				5.09	4.63		6.38	6.34

TABLE A2
(continued)

	Granite			Syenite	Granite			
Sample	DB-17	DB-19	DB-25	DB-26C	DB-29	DB-30	DB-32	DB-33
SiO_2 (%)	74.41	73.31	76.72	63.19	73.58	76.40	74.97	74.26
TiO_2	0.28	0.30	0.21	0.76	0.26	0.10	0.27	0.23
Al_2O_3	12.97	12.83	12.28	16.33	12.85	12.68	12.34	12.45
$Fe_2O_3{}^*$	2.86	3.46	2.14	4.78	3.08	1.16	2.77	2.61
MnO	0.04	0.04	0.00	0.18	0.06	0.02	0.03	0.04
MgO	0.12	0.09	0.00	0.74	0.10	0.00	0.05	0.08
CaO	0.33	0.36	0.17	2.02	0.51	0.18	0.34	0.49
Na_2O	4.27	4.23	3.39	6.00	4.38	3.27	4.10	4.22
K_2O	4.64	4.80	4.84	5.53	4.73	4.98	4.63	4.59
P_2O_5	0.05	0.06	0.06	0.24	0.07	0.10	0.03	0.04
LOI	0.19	0.49	0.58	0.48	0.39	0.67	0.58	0.20
SUM	100.17	99.96	100.39	100.25	100.00	99.56	100.11	99.21
Ni (ppm)	4	5	5	7	4	5	6	4
V	14	11	8	35	11	8	10	11
Zn	108	86	86	151	116	52	122	119
Rb	155	196	204	173	158	202	167	178
Ba	217	129	41	389	129	90	112	149
Sr	35	19	6	115	21	17	13	22
Ga	26	28	29	24	27	21	27	26
Ta			2.6	0.8	0.0	1.1		2.4
Nb	35.2	38.6	38.9	26.5	29.6	17.3	35.2	32.4
Hf			23.8	18.2		4.3		21.5
Zr	588	723	827	799	660	100	641	732
Y	62	110	73	121	64	58	75	84
Th	26.5	29.4	24.6	5.9	19.6	16.6	24.9	24.6
U	4.7	4.6	3.7	1.7	5.2	5.2	4.5	4.2
La	78.5	105.3	79.6	113.8	59.1	23.9	83.9	81.4
Ce	175.9	209.6	198.4	161.1	152.9	54.5	164.3	124.2
Pr			20.64	18.91		6.68		22.61
Nd			79.1	118.6		25.1		89.4
Sm			13.64	24.14		6.67		17.25
Eu			0.12	1.38		0.08		0.45
Gd			10.85	24.79		7.43		13.94
Tb			1.80	4.09		1.55		2.34
Dy			11.96	25.48		9.98		14.81
Ho			2.61	4.91		2.08		3.04
Er			9.13	13.90		6.47		8.90
Tm			1.53	1.83		1.01		1.38
Yb			10.59	10.86		6.39		9.66
Lu			1.53	1.48		0.91		1.47
A/NK	1.08	1.06	1.14	1.03	1.04	1.18	1.05	1.05
A/CNK	1.03	1.00	1.10	0.84	0.97	1.14	1	0.97
Eu/Eu*			0.03	0.17		0.03		0.09
$(La/Yb)_n$			5.03	7.01		2.50		5.63

Table A2

(continued)

	Granite						
Sample	DB-35	DB-36	DB-37	DB-38	DB-39	DB-41	DB-42
SiO_2 (%)	75.34	74.69	73.37	73.95	74.17	75.40	73.88
TiO_2	0.35	0.28	0.25	0.24	0.24	0.26	0.31
Al_2O_3	12.41	12.08	12.63	13.00	12.58	11.81	12.89
$Fe_2O_3{}^*$	2.01	2.87	2.91	3.00	2.98	2.94	3.35
MnO	0.04	0.05	0.04	0.05	0.06	0.05	0.05
MgO	0.03	0.08	0.08	0.08	0.08	0.09	0.08
CaO	0.29	0.55	0.40	0.48	0.50	0.36	0.15
Na_2O	4.10	4.17	4.25	4.42	4.34	3.77	3.83
K_2O	4.69	4.45	4.68	4.67	4.55	4.76	4.69
P_2O_5	0.04	0.06	0.08	0.05	0.04	0.05	0.05
LOI	0.49	0.98	0.49	0.10	0.29	0.39	0.76
SUM	99.78	100.26	99.18	100.05	99.83	99.88	100.05
Ni (ppm)	3	3	2	5	3	3	4
V	9	11	10	9	10	11	10
Zn	105	114	106	111	125	153	148
Rb	181	149	162	162	157	196	175
Ba	116	126	129	130	135	129	147
Sr	12	21	17	21	21	21	17
Ga	27	25	27	27	27	25	26
Ta		1.7				2.0	2.3
Nb	47.4	32.5	31.7	28.5	31.9	35.1	39.7
Hf		18.0				21.8	21.5
Zr	472	697	555	584	655	775	829
Y	60	62	58	62	94	82	87
Th	26.7	16.5	19.4	20.8	20.5	20.6	21.6
U	5.8	2.4	4.8	7.7	2.7	3.9	3.6
La	43.8	44.3	46.7	58.7	108.8	67.8	80.2
Ce	93.3	102.4	142.5	159.3	212.5	175.2	236.3
Pr		12.10				18.31	20.89
Nd		47.1				69.6	78.7
Sm		9.39				13.68	14.44
Eu		0.28				0.36	0.39
Gd		8.64				12.99	13.31
Tb		1.56				2.41	2.46
Dy		10.83				14.89	15.43
Ho		2.16				3.01	3.16
Er		7.21				9.26	9.37
Tm		1.19				1.43	1.47
Yb		7.64				9.54	10.75
Lu		1.19				1.44	1.51
A/NK	1.05	1.03	1.05	1.05	1.04	1.04	1.13
A/CNK	1	0.95	0.99	0.98	0.97	0.98	1.11
Eu/Eu*		0.09				0.08	0.09
$(La/Yb)_n$		3.88				4.75	4.99

$Fe_2O_3{}^*$ = total Fe as Fe_2O_3; A/NK = Al_2O_3/(Na_2O + K_2O) (mol%); A/CNK = Al_2O_3/(CaO + Na_2O + K_2O) (mol%).

References

Beard, J. S., 1995, Experimental, geological, and geochemical constraints on the origin of low-K silicic magmas in oceanic arcs: Journal of Geophysical Research, v. 100, n. B8, p. 15,593–15,600, http://dx.doi.org/10.1029/95JB00861

Bogdanov, N. A., Khain, V. E., Rozen, O. M., Shipilov, E. V., Vernikovsky, V. A., Drachev, S. S., Kostyuchenko, S. L., Kuzmichev, A. B., and Sekretov, S. B., 1998, Explanatory Note and Tectonic Map of the Kara and Laptev Seas and Northern Siberia at a Scale of 1:2,500,000: Moscow, Russian Academy of Sciences, Institute of Lithosphere of Marginal and Interior Seas, 127 p.

Bonin, B., 2007, A-type granites and related rocks: Evolution of a concept, problems and prospects: Lithos, v. 97, n. 1–2, p. 1–29, http://dx.doi.org/10.1016/j.lithos.2006.12.007

Brown, P. E., and Becker, S. M., 1986, Fractionation, hybridisation and magma mixing in the Kialineq center, East Greenland: Contributions to Mineralogy and Petrology, v. 92, n. 1, p. 57–70, http://dx.doi.org/10.1007/BF00373963

Chaudhri, N., Kauri, P., Okrusch, M., and Schimrosczyk, N., 2003, Characterisation of the Dabla granitoids, North Khetri copper belt, Rajasthan, India: Evidence of bimodal anorogenic felsic magmatism: Gondwana Research, v. 6, n. 4, p. 879–895, http://dx.doi.org/10.1016/S1342-937X(05)71032-7

Civetta, L., D'Antonio, M., Orsi, G., and Tilton, G. R., 1998, The geochemistry of volcanic rocks from Pantelleria Island, Sicily Channel: Petrogenesis and characteristics of the mantle source region: Journal of Petrology, v. 39, n. 8, p. 1453–1491, http://dx.doi.org/10.1093/petroj/39.8.1453

Clemens, J. D., Holloway, J. R., and White, A. J. R., 1986, Origin of an A-type granite: Experimental constraints: American Mineralogist, v. 71, n. 3–4, p. 317–324.

Collins, W. J., Beams, S. D., White, A. J. R., and Chappell, B. W., 1982, Nature and origin of A-type granites with particular reference to Southeastern Australia: Contributions to Mineralogy and Petrology, v. 80, n. 2, p. 189–200, http://dx.doi.org/10.1007/BF00374895

Cox, K. G., Bell, J. D., and Pankhrust, R. J., 1979, The interpretation of igneous rocks: London, George Allen & Unwin, 450 p.

De la Roche, H., Leterrier, J., Grandclaude, P., and Marchal, M., 1980, A classification of volcanic and plutonic rocks using R_1-R_2 diagram and major element analyses: Its relationships with current nomenclature: Chemical Geology, v. 29, n. 1–4, p. 183–210, http://dx.doi.org/10.1016/0009-2541(80)90020-0

Derbeko, I. M., 2012, Bimodal volcano-plutonic complexes in the frame of Eastern Member of Mongol-Okhotsk orogenic belt, as a proof of the time of final closure of Mongol-Okhotsk basin, *in* Stoppa, F., editor, Updates in Volcanology—A Comprehensive Approach to Volcanological Problems: Rijeka, InTech-www.intechopen.com, p. 99–124, http://dx.doi.org/10.5772/2328124

Droop, G. T. R., 1987, A general equation for calculating Fe^{3+} concentrations in ferromagnesian silicates and oxides from microprobe analyses, using stoichiometric criteria: Mineralogical Magazine, v. 51, p. 431–435, http://dx.doi.org/10.1180/minmag.1987.051.361.10

Eby, G. N., 1990, The A-type granitoids: A review of their occurrence and chemical characteristics and speculations on their petrogenesis: Lithos, v. 26, n. 1–2, p. 115–134, http://dx.doi.org/10.1016/0024-4937(90)90043-Z

——— 1992, Chemical subdivision of the A-type granitoids: Petrogenetic and tectonic implications: Geology, v. 20, n. 7, p. 641–644, http://dx.doi.org/10.1130/0091-7613(1992)020⟨0641:CSOTAT⟩2.3.CO;2

Frost, B. R., Barnes, C. G., Collins, W. J., Arculus, R. J., Ellis, D. J., and Frost, C. D., 2001, A geochemical classification for granitic rocks: Journal of Petrology, v. 42, n. 11, p. 2033–2048, http://dx.doi.org/10.1093/petrology/42.11.2033

Frost, C. D., and Frost, B. R., 2011, On ferroan (A-type) granitoids: their compositional variability and modes of origin: Journal of Petrology, v. 52, n. 1, p. 39–53, http://dx.doi.org/10.1093/petrology/egq070

Hawthorne, F. C., and Oberti, R., 2007, Classification of the amphiboles: Reviews in Mineralogy and Geochemistry, v. 67, n. 1, p. 55–88, http://dx.doi.org/10.2138/rmg.2007.67.2

Hofmann, M., Linnemann, U., Rai, V., Becker, S., Gartner, A., and Sagawe, A., 2011, The India and South China cratons at the margin of Rodinia-synchronous Neoproterozoic magmatism revealed by LA-ICP-MS zircon analyses: Lithos, v. 123, n. 1–4, p. 176–187, http://dx.doi.org/10.1016/j.lithos.2011.01.012

Jahn, B. M., Litvinovsky, B. A., Zanvilevich, A. N., and Reichow, M., 2009, Peralkaline granitoid magmatism in the Mongolian-Transbaikalian Belt: Evolution, petrogenesis and tectonic significance: Lithos, v. 113, n. 3–4, p. 521–539, http://dx.doi.org/10.1016/j.lithos.2009.06.015

Kalimulin, S. M., 1968, Geological setting and mineral resources in the midstream of the Kherulen river basin (sheets L-49-II, III, IV,VIII): Report of geologic mapping at the scale of 1:200 000 carried out under the contract No. 1497 from April 1966, by party No. 5 of the Central Geologic exploration expedition No. 15 of the Office of External Relations of the Ministry of Geology of the SSSR in 1966-1967 (in Russian).

Kerr, A., and Fryer, B. J., 1993, Nd isotope evidence for crust–mantle interaction in the generation of A-type granitoid suites in Labrador, Canada: Chemical Geology, v. 104, n. 1–4, p. 39–60, http://dx.doi.org/10.1016/0009-2541(93)90141-5

Kuzmin, M. I., Yarmolyuk V. V., and Kravchinsky, V. A., 2010, Phanerozoic hot spot traces and paleogeographic reconstructions of the Siberian continent based on interaction with the African large low shear velocity province: Earth-Science Reviews, v. 102, n. 1–2, p. 29–59, http://dx.doi.org/10.1016/j.earscirev.2010.06.004

Liégeois, J. P., Navez, J., Hertogen, J., and Black, R., 1998, Contrasting origin of post-collisional high-K calc-alkaline and shoshonitic versus alkaline and peralkaline granitoids; the use of sliding normalization: Lithos, v. 45, n. 1–4, p. 1–28, http://dx.doi.org/10.1016/S0024-4937(98)00023-1

Litvinovsky, B. A., Zanvilevich, A. N., Wickham, S. M., and Steele, I. M., 1999, Origin of syenite magmas in A-type granitoid series: syenite-granite series from Transbaikalia: Petrology, v. 7, n. 5, p. 459–481.
Ludwig, K. R., 2001, User's manual for Isoplot/Ex v. 2.49. A geochronological toolkit for Microsoft Excel: Berkeley Geochronological Center Special Publication 1a, 55 p.
Lynch, D. J., Musselman, T. E., Gutmann, J. T., and Patchett, P. J., 1993, Isotopic evidence for the origin of Cenozoic volcanic rocks in the Pinacate Volcanic Field, Northwestern Mexico: Lithos, v. 29, n. 3–4, p. 295–302, http://dx.doi.org/10.1016/0024-4937(93)90023-6
Marks, M., and Markl, G., 2001, Fractionation and assimilation processes in the alkaline augite syenite unit of the Ilímaussaq intrusion, South Greenland, as deduced from phase equilibria: Journal of Petrology, v. 42, n. 10, p. 1947–1969, http://dx.doi.org/10.1093/petrology/42.10.1947
Owen, J. V., 2012, Double corona structures in 18th century porcelain (1st patent Bow, London, mid-1740s): A record of partial melting and subsolidus reactions: Canadian Mineralogist, v. 50, n. 5, p. 1255–1264, http://dx.doi.org/10.3749/canmin.50.5.1255
Patiňo Douce, A. E., 1997, Generation of metaluminous A-type granites by low-pressure melting of calc-alkaline granitoids: Geology, v. 25, n. 8, p. 743–746, http://dx.doi.org/10.1130/0091-7613(1997)025⟨0743:GOMATG⟩2.3.CO;2
Pearce, J. A., Harris, N. B., and Tindle, A. G., 1984, Trace element discrimination diagrams for the tectonic interpretation of granitic rocks: Journal of Petrology, v. 25, n. 4, p. 956–983, http://dx.doi.org/10.1093/petrology/25.4.956
Peccerillo, R., and Taylor, S. R., 1976, Geochemistry of Eocene calc-alkaline volcanic rocks from the Kastamonu area, northern Turkey: Contributions to Mineralogy and Petrology, v. 58, n. 1, p. 63–81, http://dx.doi.org/10.1007/BF00384745
Platt, R. G., 1996, Nepheline syenite complexes-an overview, *in* Mitchell, R. H., editor, Undersaturated alkaline rocks: mineralogy, petrogenesis and economic potential: Mineralogical Association of Canada Short Course Notes, v. 24, p. 63–99.
Rapp, R. P., and Watson, E. B., 1995, Dehydration melting of metabasalt at 8-32 kbar: Implications for continental growth and crust-mantle recycling: Journal of Petrology, v. 36, n. 4, p. 891–931, http://dx.doi.org/10.1093/petrology/36.4.891
Reichow, M. K., Litvinovsky, B. A., Parrish, R. R., and Saunders, A. D., 2010, Multi-stage emplacement of alkaline and peralkaline syenite–granite suites in the Mongolian–Transbaikalian Belt, Russia: Evidence from U-Pb geochronology and whole rock geochemistry: Chemical Geology, v. 273, n. 1–2, p. 120–135, http://dx.doi.org/10.1016/j.chemgeo.2010.02.017
Ritchie, N. W. M., Newbury, D. E., and Davis, J. M., 2012, EDS measurements of X-ray intensity at WDS precision and accuracy using a silicon drift detector: Microscopy and Microanalysis, v. 18, n. 4, p. 892–904, http://dx.doi.org/10.1017/S1431927612001109
Robinson, P., Spear, F. S., Schumacher, J. C., Laird, J., Klein, C., Evans, B. W., and Doolan, B. L., 1982, Phase relations of metamorphic amphiboles, *in* Veblen, D. R., and Ribbe, P. H., editors. Amphiboles: petrology and experimental phase relations: Reviews in Mineralogy and Geochemistry, v. 9B, p. 1–227.
Ronga, F., Lustrino, M., Marzoli, A., and Melluso, L., 2010, Petrogenesis of a basalt-comendite-pantellerite rock suite: the Boseti Volcanic Complex (Main Ethiopian Rift): Mineralogy and Petrology, v. 98, n. 1–4, p. 227–243, http://dx.doi.org/10.1007/s00710-009-0064-3
Sengör, A. M. C., Natal'in, B. A., and Burtman, V. S., 1993, Evolution of Altaid tectonic collage and Paleozoic crustal growth in Eurasia: Nature, v. 364, p. 299–307, http://dx.doi.org/10.1038/364299a0
Shellnutt, J. G., Bhat, G. M., Wang, K. L., Brookfield, M. E., Dostal, J., and Jahn, B. M., 2012, Origin of the silicic volcanic rocks of the Early Permian Panjal Traps, Kashmir, India: Chemical Geology, v. 334, p. 154–170, http://dx.doi.org/10.1016/j.chemgeo.2012.10.022
Sircombe, K. N., 2004, AGEDISPLAY: an EXCEL workbook to evaluate and display univariate geochronological data using binned frequency histograms and probability density distributions: Computers and Geosciences, v. 30, n. 1, p. 21–31, http://dx.doi.org/10.1016/j.cageo.2003.09.006
Sisson, T. W., Ratajevski, K., Hankins, W. B., and Glazner, A. F., 2005, Voluminous granitic magmas from common basaltic source: Contributions to Mineralogy and Petrology, v. 148, n. 6, p. 635–661, http://dx.doi.org/10.1007/s00410-004-0632-9
Stacey, J. S., and Kramers, J. D., 1975, Approximation of terrestrial lead evolution by a two-stage model: Earth and Planetary Science Letters, v. 26, n. 2, p. 207–221, http://dx.doi.org/10.1016/0012-821X(75)90088-6
Sun, S. S., and McDonough, W. F., 1989, Chemical and isotopic systematics of oceanic basalts: implications for mantle composition and processes, *in* Saunders, A. D., and Norry, M. J., editors, Magmatism in the Ocean Basins: Geological Society, London, Special Publications, v. 42, p. 313–345, http://dx.doi.org/10.1144/GSL.SP.1989.042.01.19
Taylor, R. P., Strong D. F., and Fryer B. J., 1981, Volatile control of contrasting trace element distributions in peralkaline granitic and volcanic rocks: Contributions to Mineralogy and Petrology, v. 77, n. 3, p. 267–271, http://dx.doi.org/10.1007/BF00373542
Thorpe, R. S., and Tindle, A. G., 1992, Petrology and petrogenesis of a Tertiary bimodal diorite-peralkaline/subalkaline trachyte-rhyolite dyke association from Lundy, Bristol Channel, UK: Geological Journal, v. 27, n. 2, p. 101–117, http://dx.doi.org/10.1002/gj.3350270202
Turner, S. P., Foden, J. D., and Morrison, R. S., 1992, Derivation of some A-type magmas by fractionation of basaltic magma: An example from the Padthaway Ridge, South Australia: Lithos, v. 28, n. 2, p. 151–179, http://dx.doi.org/10.1016/0024-4937(92)90029-X
Vernikovsky, V. A., Kazansky, A. Y., Matushkin, N. Yu., Metelkin, D. V., and Sovetov, J. K., 2009, The geodynamic evolution of the folded framing and the western margin of the Siberian craton in the Neoproterozoic: geological, structural, sedimentological, geochronological, and paleomagnetic data: Russian Geology and Geophysics, v. 50, n. 4, p. 380–393, http://dx.doi.org/10.1016/j.rgg.2009.03.014
Whalen, J. B., Currie, K. L., and Chappell, B. W., 1987, A-type granites: geochemical characteristics,

discrimination and petrogenesis: Contributions to Mineralogy and Petrology, v. 95, n. 4, p. 407–419, http://dx.doi.org/10.1007/BF00402202

Wilhem, C., Windley, B. F., and Stampfli, G. M., 2012, The Altaids of Central Asia: A tectonic and evolutionary innovative review: Earth Science Reviews, v. 113, n. 3–4, p. 303–341, http://dx.doi.org/10.1016/j.earscirev.2012.04.001

Wu, F. Y., Sun, D. Y., Li, H. M., Jahn, B. M., and Wilde, S. A., 2002, A-type granites in Northeastern China: age and geochemical constraints on their petrogenesis: Chemical Geology, v. 187, n. 1–2, p. 143–173, http://dx.doi.org/10.1016/S0009-2541(02)00018-9

Yarmolyuk, V. V., and Kovalenko, V. I., 1991, Rift magmatism of active continental margins and its ore potential: Moscow, Nauka, 263 p. (in Russian).

Yarmolyuk, V. V., and Kuzmin, M. I., 2011, Rifting and silicic large igneous provinces of the Late Paleozoic–Early Mesozoic in the Central Asia: Large Igneous Provinces Commission, http://www.largeigneousprovinces.org/11dec

Yarmolyuk, V. V., Kovalenko, V. I., Salnikova, E. B., Budnikov, S. V., Kovach, V. P., Kotov, A. B., and Ponomarchuk, V. A., 2002, Tectono-magmatic zoning, magma sources, and geodynamic of the Early Mesozoic Mongolo-Transbaikalian magmatic area: Geotectonics, v. 36, p. 293–311.

Yavuz, F., 2007, WinAmphcal: A Windows program for the IMA-04 amphibole classification: Geochemistry Geophysics Geosystems, v. 8, n. 1, Q01004, 12 p., http://dx.doi.org/10.1029/2006GC001391

Yu, X., Yang, S.-F., Chen, H.-L., Chen, Z.-Q., Li, Z.-L., Batt, G. E., and Li, Y.-Q., 2011, Permian flood basalts from the Tarim Basin, Northwest China: SHRIMP zircon U–Pb dating and geochemical characteristics: Gondwana Research, v. 20, n. 2–3, p. 485–497, http://dx.doi.org/10.1016/j.gr.2010.11.009

Zhao, J. X., Shiraishi, K., Ellis, D. J., and Sheraton, J. W., 1995, Geochemical and isotopic studies of syenites from the Yamato Mountains, East Antarctica: implications for the origin of syenitic magmas: Geochimica and Cosmochimica Acta, v. 59, n. 7, p. 1363–1382, http://dx.doi.org/10.1016/0016-7037(95)00050-A

Zindler, A., and Hart, S., 1986, Chemical geodynamics: Annual Review of Earth Planetary Sciences, v. 14, p. 493–571, http://dx.doi.org/10.1146/annurev.ea.14.050186.002425